

Please note that this paper is a non-peer reviewed preprint submitted to EarthArXiv. It has been submitted to *Geophysical Research Letters* for peer review.

The influence of sea-level curves on modeled marine terrace sequences

Gino de Gelder¹, Julius Jara-Muñoz², Daniel Melnick³, David Fernández-Blanco¹, Hélène Rouby¹, Kevin Pedoja⁴, Rolando Armijo¹ and Robin Lacassin¹

¹Institut de Physique du Globe de Paris, Sorbonne Paris Cité, Univ. Paris Diderot, UMR 7154 CNRS, F-75005 Paris, France.

²Institut für Erd- und Umweltwissenschaften, Universität Potsdam, Karl-Liebknecht-Strasse 24, 14476 Potsdam, Germany.

³Instituto de Ciencias de la Tierra, Universidad Austral de Chile, 567 Valdivia, Chile

⁴Laboratoire de Morphodynamique Continentale et Côtière, CNRS, Université de Caen, 14000 Caen, France.

Corresponding author: Gino de Gelder (gelder@ipgp.fr)

Key Points:

- A landscape evolution model allows us to constrain the chronology of marine terraces, uplift rates and best-fitting sea-level curves
- The sea-level curve fit between observed and modeled terrace morphology depends on the time-span and/or uplift rate
- Eustatic sea levels of successive highstands are particularly influential to generate typical Quaternary terrace staircase sequences

Abstract

Widespread sequences of uplifted marine terraces express multi-scale climatic and tectonic processes, but their analysis is typically biased by the considered sea-level curve. Here we explore the influence of Quaternary sea-level (SL) curves on the geometry of the marine terrace sequence at Xylokastro (Corinth Rift) using a numerical model of sea-cliff erosion. Modeling the young, rapidly uplifting sequence (<240 ka; ~1.5 mm/yr;) allows us to constrain terrace ages, model parameters and best-fitting SL curves. While SL curves based on ages of coastal index point (corals) achieve lower misfits than hydraulic-model based curves at Xylokastro, the latter SL curves are better for modeling coasts that rise slowly (~0.2 mm/yr) over longer timescales (2.6 Ma). Our study emphasizes the importance of eustatic highstand elevations to estimate uplift rates from staircase marine terrace sequences. Accurately modeling such sequences can be crucial in assessing primary climatic and tectonic contributors to Quaternary coastal evolution.

Plain Language Summary

Marine terrace sequences are landforms observed along coastlines worldwide. They form over thousands to millions of years and are important in quantifying both uplift rates of tectonically active areas and global sea-level history, described by graphs called sea-level curves. The main goal of our study is to present a novel approach that allows us to 1) quantify terrace ages and uplift rates better, and 2) to distinguish which sea-level curves can better reproduce marine terrace sequences. We do this by using 2D numerical simulations to calculate the way in which the shape of a marine terrace sequence evolves. First we test the young, rapidly uplifting sequence in Xylokastro, Greece (240,000 years; 1.5 mm/year), for which curves based on fossilized corals fit best with observations. Then we test older, slower uplifting sequences (2.6 million years; 0.2 mm/year), for which curves based on oxygen/salinity levels of marine sediments fit best with observations. Our results show that the shape of a marine terrace sequence can provide important information on the elevation of past sea-levels. Our approach can be used for other marine terraces worldwide, and may be a crucial way to improve our understanding of both tectonic processes and global sea level history.

1 Introduction

Quantifying glacio-eustatic sea-level (SL) variations is fundamental to estimate global ice-sheet volumes and their spatio-temporal response to climate change (e.g. Chappell and Shackleton, 1986; Lambeck et al., 2002, 2014), and quantifying coastal uplift rates is essential for assessing tectonic dynamics and estimating seismic hazard (e.g. Merritts and Bull, 1989; Shaw et al., 2008). The majority of the world's coastline exposes sequences of fossil strandlines (Pedoja et al., 2011; 2014) that result from the interplay between tectonic uplift, glacio-eustatic SL variations and glacio-isostasy (e.g. Bradley, 1958; Lajoie, 1986, Anderson et al., 1999). These markers of past SL position reflect global to regional tectonic/climatic processes since the Paleogene (Yamato et al., 2013; Henry et al., 2014; Pedoja et al., 2014), and are often expressed as marine terrace sequences. Marine terraces are fossil rocky shore platforms formed by coastal erosion, occasionally covered by a thin layer of coastal sediments and bounded inland by a fossil sea-cliff (e.g. Anderson et al., 1999).

A main challenge in studying marine terraces is to constrain their ages, therefore several studies have used modeling strategies to match undated terraces to Quaternary SL highstands,

using statistical metrics (e.g. Zeuner, 1952; Bowles and Cowgill, 2012; Roberts et al., 2013) or landscape evolution models (e.g. Quarta et al., 2010; Melnick, 2016; Jara-Muñoz et al., 2017). These studies generally rely on a single SL curve, but the choice of SL curve may introduce significant uncertainties: highstand estimates range in age by ~ 20 ka and sea-level elevation by ~ 30 meters (Fig. 1). These uncertainties may lead to significant biases (Caputo, 2007). Here we propose a novel approach to model the development and age of marine terraces by investigating the influence of SL curves on marine terrace sequences. We first apply our model to the well-preserved staircase sequence of Xylokaastro (Corinth Rift, Greece) using 14 SL curves. Then, we model the SL curve signature of the change from dominantly 40 ka to 100 ka climate cycles at ~ 1250 -700 ka, known as Mid-Pleistocene Transition (MPT) (Clark et al., 2006), on a hypothetical coastal sequence using 4 SL curves that cover >2.6 Ma. Whereas Husson et al. (2018) focused on the impact of the MPT on constructional coral reef terraces, our study is the first attempt to analyze its signature on rocky-coast erosive marine terraces. The combined MPT and Xylokaastro case studies allow us to explore the intrinsic relation between terrace sequence morphology and Quaternary SL cycles on a range of timescales.

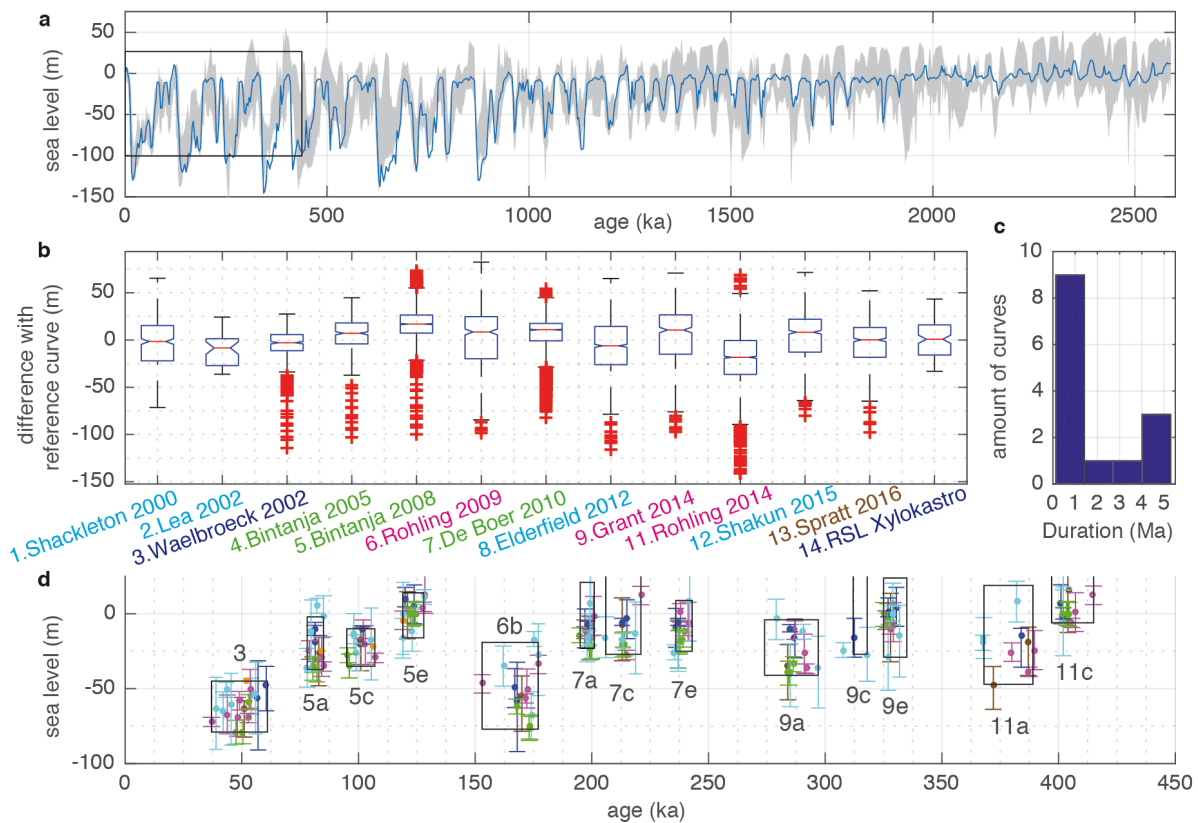


Figure 1. Compilation of selected SL curves. **(a)** The equatorial Pacific curve of Bates et al. (2014; curve 10) with the envelope of all other curves of our compilation in grey. **(b)** Boxplot of absolute differences in SL elevation between the Bates et al. (2014) curve and the other curves. Colors refer to the methodology used to produce each curve (see Table S1 and methods). Blue boxes span the 25-75% percentiles, red line the median, black lines the 95% percentiles, red crosses indicate outliers and notches indicate, with 95% confidence, if true medians are the same.

(c) Histogram of SL-curve duration (d) Elevation of SL highstands with error bars. Numbers are Marine Isotope Stages (MIS) and letters are substages as defined by Railsback et al. (2015).

2 The coastal sequence at Xylokaastro

The sequence of marine terraces at Xylokaastro (Fig. 2a) is located on the SE Corinth Rift (Greece). High uplift rates of ~ 1.3 mm/yr (Armijo et al., 1996), low sub-aerial erosion rates and thin cover of cemented coastal deposits have resulted in a well-preserved sequence of 13 marine terraces (e.g. Dufaure & Zamanis, 1979; Keraudren & Sorel 1987; Armijo et al., 1996; De Gelder et al., 2017). The terrace sequence extends over an area of $\sim 3 \times 3$ km, culminating at an elevation of ~ 400 m (Fig. 2a), and span the last ~ 240 ka. The terraces were previously named after local towns (see Armijo et al., 1996), but herein we assign a simpler name designation of TH (Holocene terrace) and T1-T12 (Fig. 2a). The T7 (New Corinth; ~ 175 m elevation) and T11 (Old Corinth; ~ 320 m elevation) terraces have been dated using both U/Th on solitary corals (Collier et al., 1992; Dia et al., 1997; Leeder et al., 2005), and IcPD dating of *Pecten* (Pierini et al., 2016). These studies correlate T7 and T11 to the Marine Isotope Stage (MIS) 5e (~ 125 ka) and MIS 7e (~ 240 ka) highstands, respectively. An inactive alluvial fan at ~ 200 - 230 m elevation caps T8 and T9, hindering our map of terraces in this ~ 0.5 km² area (Fig. 2a).

3 Methods

3.1 Landscape Evolution Model

We use a Landscape Evolution Model (LEM) based on the wave erosion and wave energy dissipation model formulated by Sunamura (1992), and further developed by Anderson et al. (1999). The model simulates the evolution of rocky coasts by retreat of a sea-cliff, driven by wave erosion and resulting in the genesis of a rocky shore platform. The model assumes that the vertical seabed erosion rate is a linear function of the rate of wave energy dissipation against the seabed (Sunamura, 1992). The energy available at the sea-cliff to drive horizontal erosion is defined by the far-field wave energy remaining after wave energy dissipation (Anderson et al., 1999). The water depth profile dictates the spatial pattern of dissipation rate, exponentially increasing landwards as the water depth decreases. We use a 2D model setup formed by a planar shelf of given slope and assume that the rate of rock uplift is uniform. Cliff retreat starts at an initial rate and evolves as the platform is carved during sea-level oscillations, which depends on the SL curve. Detailed description and equations can be found in Anderson et al. (1999).

3.2 Sea-Level Curves

3.2.1 Glacio-Eustatic Sea-Level Curves

Glacio-eustasy is the dominant long-term mechanism driving the relative SL changes observed during the Quaternary (Bloom, 1971). Long-term climatic cycles drive the periodic growth and decay of large ice-sheets, associated with global (eustatic; Suess, 1888) sea level rise and fall. We systematically selected glacio-eustatic sea-level (GESL) curves from literature that cover at least the last 3 major glacial cycles (~ 350 ka), and are based on data with a temporal resolution of < 3 ka (Table S1). For SL curves derived from oxygen isotope ratios ($\delta^{18}O$), we selected those separating temperature contribution from glacio-eustatic contribution to the $\delta^{18}O$ value. Then we subdivided the 13 SL curves (Table S1, Fig. 1) into curves that; (i) use another

proxy than $\delta^{18}\text{O}$ to estimate sea temperature variations (light blue, Fig. 1); (ii) use a regression analysis to fix $\delta^{18}\text{O}$ curves to relative SL estimates from corals (dark blue, Fig. 1); (iii) are based on global ice-sheet modeling (green, Fig. 1); (iv) are based on hydraulic models of water exchange between an evaporative sea and the ocean (pink, Fig. 1); and (v) results from principle component analysis (PCA) of 7 other curves (brown, Fig. 1). More details are given in Table S1.

3.2.2 Relative Sea-Level Curve

Strong local departures from average eustatic SL occur in response to the buildup and retreat of ice sheets because of Glacial Isostatic Adjustment (GIA) (e.g. Bloom, 1967; Walcott, 1972, Lambeck, 1995). Using the CALSEA program and the ice models developed at the Australian National University (e.g. Nakada and Lambeck, 1987; Johnston, 1993; Lambeck et al., 2003, 2012), we evaluated the amplitude that can locally be reached by the GIA effect on relative sea level. The distribution of ice history in the different ice-sheets is only well-constrained over the last glacial cycle (~ 130 ka; Lambeck et al. 2010, 2014, 2017), for which we calculated the relative sea-level GIA effect at Xylokaastro. The ANU models include all deformational, gravitational and rotational changes induced by the buildup and retreat of ice-sheets and are constructed by inversion of globally distributed, direct observational data of relative SL. We adopted the same ice sheet approximations and Earth model parameters as Simms et al. (2015) and thus expect errors of same order of magnitude (~ 5 m).

3.3 Modeling the coastal sequence at Xylokaastro

We constructed a representative cross-section of the Xylokaastro terraces to compare with the LEM simulated topography, by calculating average (i) shoreline angle elevations, (ii) terrace widths, (iii) terrace slopes and (iv) the modern rocky shore platform width. To determine shoreline angles, the intersection between the marine terrace and its associated fossil sea-cliff, we used a 2-m resolution Digital Surface Model (DSM) developed from Pleiades satellite imagery (De Gelder et al., 2015, 2017). From the DSM we calculated 100-m-wide swath profiles perpendicular to the fossil sea-cliff and determined the shoreline angle position and elevation using the fixed-slope method of TerraceM (Jara-Muñoz et al., 2016). We used the maximum swath profile topography and the modern sea-cliff slope angle of $39^\circ \pm 10^\circ$ (De Gelder et al., 2017) as a proxy for the slope of the paleo sea-cliff (Dataset S1). To approximate the terrace average width we used the distance between two successive shoreline angles (Fig. S1), since sub-aerial erosion of the paleo-cliffs has reduced the original terrace-width since they emerged. To estimate terrace slopes, we used the average slope of the modern terrace as less-eroded proxies for their older counterparts. To estimate the outer limit of the modern rocky shore platform, we assume that it has largely been carved during Holocene sea-level rise. Before ~ 12 ka (Moretti et al., 2003) the Corinth Gulf was a lake, its water exchange with the open sea limited by the 62 m deep Rion sill (Perissoratis et al., 2000). Assuming Holocene terrace carving started 12 ka at 62 m depth, and given an uplift rate of ~ 1.3 mm/yr (Armijo et al., 1996), the present depth contour of -46 m should approximately represent the outer limit of the modern rocky shore platform (Fig. S1).

We tied the cross-section shoreline angles of the dated T7 and T11 terraces to the shoreline angles formed during the MIS 5e (~ 125 ka) and MIS 7e (~ 240 ka) highstands in the LEM. We fixed LEM uplift rates to reproduce the observed average shoreline angle elevations,

and varied initial erosion rate and initial shelf slope with steps of 0.1 m/yr and 0.25°, respectively. This allowed us to select the best-fitting pair of values that resulted in the lowest Root-Mean-Squared (RMS) misfit on both ~125 and ~240 ka timescales. Our models used time steps of 200 years to match the highest resolution GESL curve we modeled (Table S1), and a spatial resolution of 2 m to match our DSM. In the modeling, we assumed that the SL in Corinth did not get lower than the Rion sill (62 m depth) during the past 240 ka. We used a wave height of 3 m, based on the highest waves recorded between 2010-2015 at the Gulf of Corinth with AVISO satellite altimetry measurements (Fig. S2). Sensitivity tests for wave height and sill depth show that those parameters do not strongly affect our results (Fig. S2).

3.4 Modeling the Mid-Pleistocene Transition

We modeled the formation of marine terraces sequences over the whole Quaternary (2.6-0 Ma) using the four longest GESL curves of our compilation (Bintanja & Van de Wal, 2008; De Boer et al., 2010, Bates et al., 2014, Rohling et al., 2014). In our modeling strategy, we used a relatively low initial slope of 4° and an uplift rate of 0.1 mm/yr, since sustained uplift and terrace preservation over such time-scales is more likely to occur on gently-sloping and slowly uplifting coastlines (Pedoja et al., 2014). We used an initial sea-cliff erosion rate of 0.6 m/yr, consistent with our average estimate for Corinth (Fig. 2c), and included a 0.1 m²/yr sub-aerial cliff diffusion rate to obtain a more realistic sequence morphology over this timescale.

4 Results

4.1 Modeling the coastal sequence at Xylokaastro

The systematic comparison of the observed topography in the Xylokaastro marine terraces sequence and their modeled topography allows us to assess possible age ranges for undated terraces (Fig. 2b), quantify the governing parameters of terrace formation (Fig. 2c-e), and evaluate the best-fitting SL curves by means of the amount of terraces reproduced and the RMS misfit (Figs. 2f and 2g). When correlating the elevations of modeled shoreline angles to the nearest shoreline angles (Fig. S3), different SL curves lead to different terrace age estimates (Fig. 2b). Most curves lead to a chrono-stratigraphy in which T2 was formed during MIS 5a (~70-85 ka), T3 during MIS 5a or MIS 5c (~92-107 ka), T4 and T5 during MIS 5c, T6 and T7 during MIS 5e (~115-128 ka), T9 during MIS 7a (~190-205 ka), T10 during MIS 7a or 7c (~210-225 ka) and T11 during MIS 7e (~235-242 ka). T1 and T8 were reproduced by only 2 and 3 SL curves respectively, but relative to the other terraces would logically have an age of MIS 5a or younger (T1), and MIS 8 or MIS 9a (T8).

The amount of terraces reproduced by the different curves varies strongly on both ~125 ka (2-7 terraces) and ~240 ka (4-10 terraces) timescales, but none of the selected curves could recreate the total observed number of terraces (Fig. 2f). The highest number of terraces for the last ~125 ka and ~240 ka result from the curves with the highest temporal resolution (curves 6, 10 in Fig. 2f; Fig. S4) and relatively high interstadial highstands (curves 1, 8 and 12 in Fig. 2f; Fig. S4), respectively. Considering RMS misfits, the SL curves that are based on corals (dark blue in Fig. 2g) consistently have a relatively low RMS misfit (<20 m) over the last ~125 ka (Fig. 2g). The curve based on PCA (brown in Fig. 2g) also has a relatively low RMS misfit (19 m), similar on both timescales, but reproduces fewer terraces than the coral-based SL curves.

Curves that use other proxies than $\delta^{18}O$ to separate temperature from glacio-eustatic components in $\delta^{18}O$ data (light blue in Fig. 2g) show both low and high RMS misfits, as well as a relatively big scatter in uplift rates. Curves based on global ice sheet modeling (green in Fig. 2f) and hydraulic models (pink in Fig. 2f) have the highest RMS misfits. On both timescales there is a correlation between the average interstadial height of the SL curve and the RMS misfit (Fig. S4).

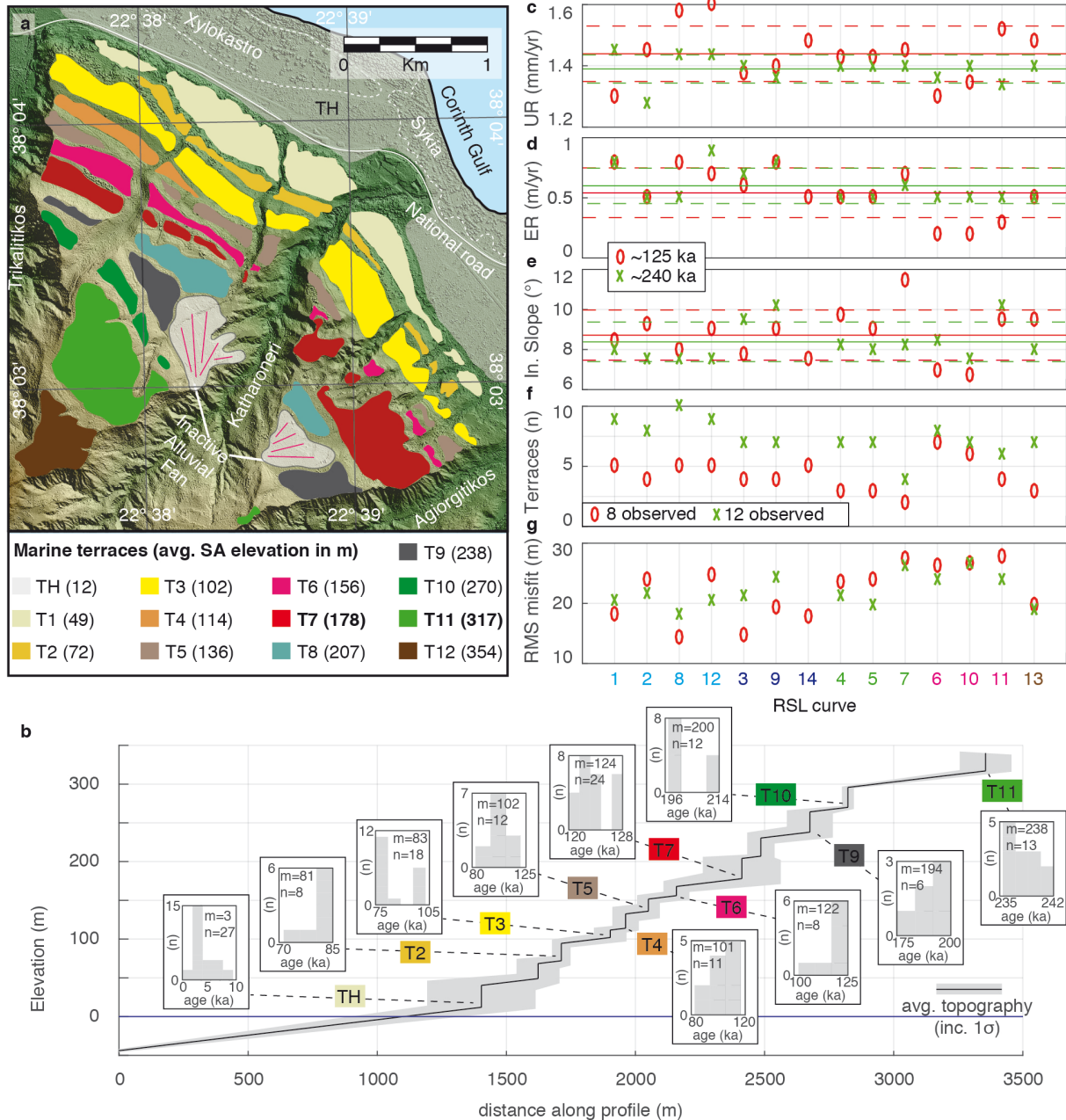


Figure 2. Modeling the marine terrace sequence at Xylokastro. **(a)** Map of the terraces. SA = shoreline angle. **(b)** The black line shows average-derived terrace topography (see methods) with 1 σ uncertainty (grey envelope) and range of possible terrace ages indicated by the different SL curves, including median age (m) and amount of curves (n) reproducing a given marine terrace

(c-g) Different parameters and outcomes resulting from finding the lowest RMS-misfit over the two time-scales. Models over 125 ka and 240 ka are shown in red and green, respectively. Numbers below plot correspond to SL-curve numbering and colors of Fig. 1. Solid and dashed lines indicate average values and 1σ uncertainty. **(c)** Uplift rates required by the different SL curves to match the correct elevations of the dated T7 (red) and T11 (green) terraces. **(d)** Erosion rate for lowest RMS-misfit result. **(e)** Initial slope for lowest RMS-misfit result. **(f)** Total number of terraces for lowest RMS-misfit result. **(g)** Lowest RMS-misfits.

4.2 Modeling the Mid-Pleistocene Transition

The lower uplift rate (0.2 mm/yr) used for the 2.6-Ma models (Fig. 3) results in fewer terraces being formed than at Xylokaastro (Fig. 2). At such uplift rates, only terraces formed during the maxima of interglacial highstands (MIS 5e, 7e etc.) are preserved. The effect of the Mid-Pleistocene Transition (MPT) is most pronounced in modeling the curve of Rohling et al. (2014), with 2 rasas (wide polygenic fossil strandlines) formed before the MPT and 5 marine terraces after the MPT (Fig. 3e). The sequences produced by the other SL curves do not show such a clear contrast before and after the MPT. The curve with the most (Bates et al., 2014) and least (Rohling et al., 2014) pronounced change in cyclicity around the MPT (spectrograms in Fig. S5), correspond to the relative least and most pronounced change in sequence morphologies, respectively (Fig. 3). Additional tests with other values for uplift rates, erosion rates and initial slope show a variety in shape of the staircase sequences (Fig. S6), but consistently result in the hydraulic curve (Rohling et al., 2014) having the lowest ratio between terraces/rasas preserved before and after the MPT.

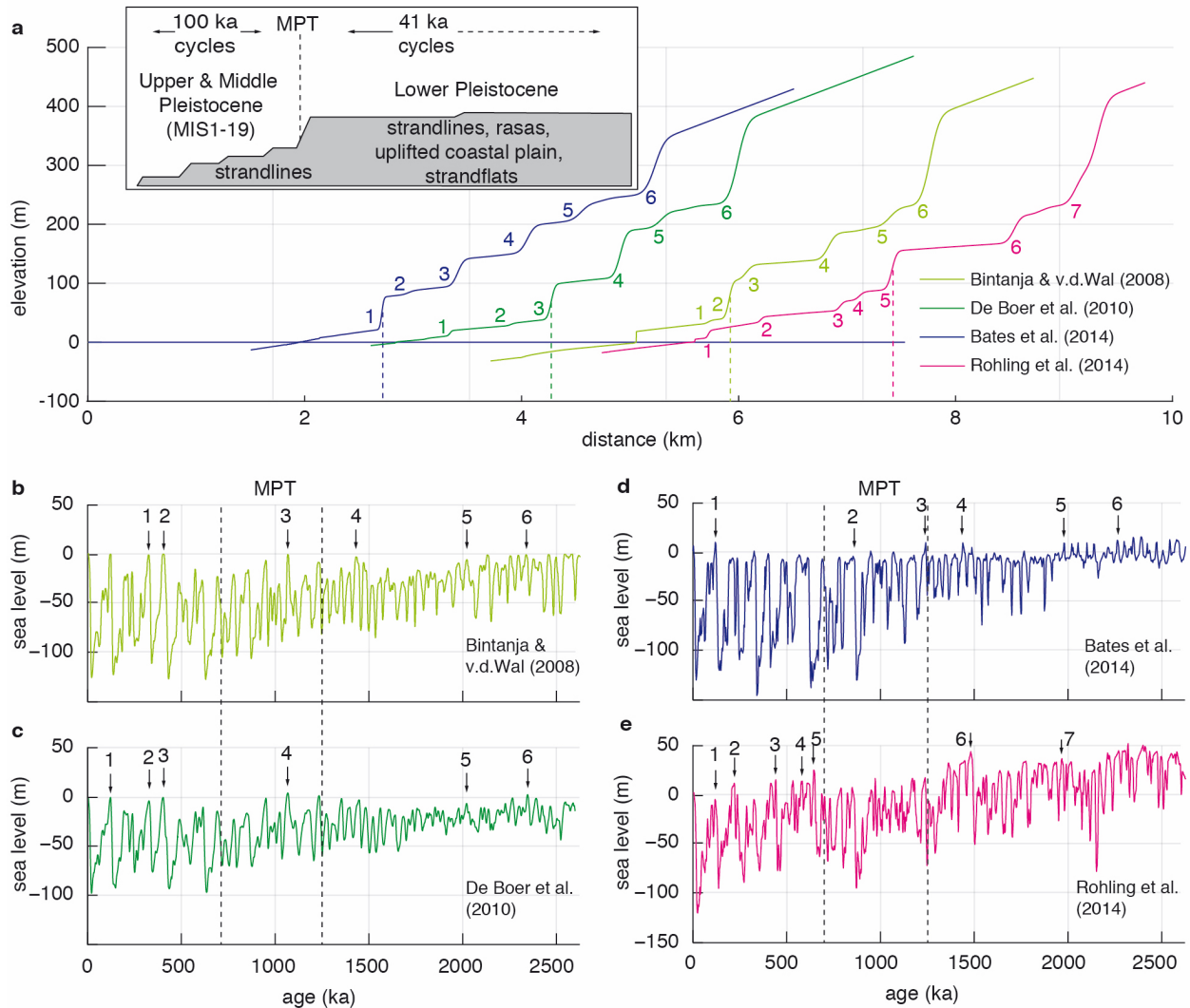


Figure 3. Model results on Quaternary (2.6 Ma) timescale. **(a)** Modeled geometry of the long-term sequences, dashed lines indicating the Mid-Pleistocene Transition (MPT). Inset shows typical morphology for a Quaternary staircase sequence, modified from Pedoja et al. (2014). **(b-e)** Modeled SL curves, with numbered arrows indicating SL highstands that result in preserved terraces in **a**.

5 Discussion

5.1 Modeling coastal sequences: the Xylokaastro lessons

Modeling tests on the Xylokaastro terrace sequence reveal the complexity of reproducing as numerous terrace levels as observed in the field and on the DSM. This might be a consequence of model assumptions and/or SL curves used. The relatively simple model used (Anderson et al., 1999) does not take into account the abrasive effect of sediments, long-shore drift, and coastal deposits forming on the terraces. Although these might all be of influence to the terrace sequence geometry, implementing such processes within our model is beyond the scope of this study, and in any model the influence of the chosen sea-level curve would remain of primary importance. Our simple model assumptions of constant uplift rate, erosion rate and

initial shelf slope are supported by the result that none of those parameters have significantly changed on both timescales (Fig. 2c-e).

Considering the limitations of the SL curves used, the temporal resolution may restrict the amount of terrace levels produced. The curves with the highest resolution (Rohling et al., 2009; Grant et al., 2014, Figs. S3 and S4) show that sharp and short duration peaks within a SL-curve can result in extra terrace levels. Detailed studies of MIS 5e show that multiple peaks may have occurred even within one highstand (e.g. Hearty et al., 2007; Pedoja et al., 2011; Murray-Wallace and Woodroffe, 2014), which is not reflected within most of the SL curves. The GIA-based RSL-curve does not fit the topography better than other curves based on coral data (Fig. 2g) suggesting that the applied GIA-correction is not sufficient to explain poor fits to the data. In general, the location of the data on which the SL curves are based (Table S1) does not appear to affect RMS-misfits at Xylokaastro. The hydraulic-model curves (Rohling et al., 2009, 2014; Grant et al., 2014) are based on Mediterranean and Red Sea data, comparatively close in location to Xylokaastro, but have relatively high RMS misfits (>24 m).

Our analysis for the Xylokaastro sequence provides clear advantages over more classic analyses that do not include modeling (e.g. Merritts and Bull, 1989; Armijo et al., 1996; Strobl et al., 2014). Using a range of different curves is essential to check the robustness of uplift rate estimates and possible correlations between undated marine terraces and SL highstands, as noted in some previous studies (e.g. Caputo, 2007; Yildirim et al., 2013; Pedoja et al., 2018a,b). Our approach expands on these studies by not only using shoreline angles and SL highstands, but using the full terrace sequence geometry and complete SL curves, i.e. taking advantage of the model prediction that higher highstands and longer periods of preceding SL rise lead to wider terraces. Such geometrical trends, with some highstands leading to wider terraces, are also observed in nature (Regard et al., 2017). Additionally, a modeling approach allows for an evaluation of parameters like erosion rates and initial slopes, and their evolution through time, with possible climatic and paleogeographic implications.

Another advantage is that we can analyze which SL curves better reproduce the geometry of a studied marine terrace sequence. It is reasonable that for the Xylokaastro sequence, curves based on coral data have lower misfits on a 125 ka than 240 ka timescale, since the data on which they are based become sparser with increasing age. The lowest RMS misfits are achieved by the SL curves that have relatively high interstadial highstands (MIS 3, 5a, 5c, 6, 7a, 7c in Fig. 1d; Fig. S4), which are the curves based on coral data (3, 9, 14), some of the curves based on other proxies to measure sea temperature (1, 8) and the PCA-based curve (13). We speculate that these curves are the most appropriate to describe SL variations to a first order degree, but their lack of temporal resolution produces too few terraces. Contrarily, the two highest-resolution hydraulic-model curves (6, 10 in Fig. 2f; Fig. S4) produce more terrace levels on the ~125 ka runs, but their high RMS misfits suggest that they are less appropriate to describe first order SL variations. Although these inferences are based on one sequence of 13 terraces, and thus the SL curves that are more credible here might not be elsewhere, similar analyses can be applied to many locations worldwide (see compilation in Pedoja et al., 2014). Such a comparison could allow for a global perspective on SL variations and best-fitting SL curves from marine terraces.

5.2 The MPT and Quaternary Evolution of Staircase Coastal Landscapes

Based on global observations of Neogene-Quaternary sequences of strandlines, Pedoja et al. (2014) suggested that the change in cyclicity frequency from 40 to 100 ka during the MPT is generally causal for a contrast between wide rasas before the MPT, and narrower and better individualized marine terraces after the MPT (inset in Fig. 3a). Within this context, modeling with low uplift rates over 2.6 Ma (Fig. 3) suggests that the SL-curves based on hydraulic models (Rohling et al., 2014) and corals (Bates et al., 2014) are the most and least successful, respectively, in recreating globally observed sequences. This is opposite to our findings for Xylokaastro. For the high uplift rates in Xylokaastro (Fig. 2) the relative difference between interglacial and interstadial highstands is more important than for the slowly uplifting models (Fig. 3), in which the elevations of interglacial highstands are the most important. Whereas coral-based curves, largely based on a dataset over the past ~125 ka, appear to describe those relative elevations of interglacial and interstadial highstands better, hydraulic based curves relying on long continuous sedimentary records appear to record interglacial highstands better over longer timespans. The opposite results for the Xylokaastro and MPT case studies hint that different types of SL curves are suitable for different timescales and/or uplift rates.

Our results imply that the patterns in highstand elevations, superposed on the change in dominant cyclicity and amplitude during the MPT, play a crucial role in the amount of terraces/rasas being formed and preserved over Quaternary timescales. For the period before the MPT, highly elevated peaks in SL can overprint multiple terraces formed during preceding highstands to develop wide rasas. After the MPT, similar elevated highstands or highstands that gradually decrease in elevation (as in Rohling et al., 2014; Fig. 3) are required to preserve numerous marine terraces with slow uplift rates. An indication for similar elevations in post-MPT interglacial highstands comes from slowly uplifted shorelines (~0.07 mm/yr) dated in Australia (Murray-Wallace, 2002, 2014), indicating that SL-highstands of interglacials over the past ~800 ka (MIS 21-19-17-15-13-11-9-7-5) were all within 2 m of present-day sea level.

Currently, only a few dated records of marine terrace sequences cover the entire Quaternary timescale (e.g. Guyomard, 1996; Meco et al., 2007). Although reliable dating of marine terrace sequences is essential, our study shows that modeling the detailed sequence morphology can already provide first order constraints on SL variations over various timescales. The rapidly increasing availability of high-resolution topography, like the Xylokaastro DSM used in this study, is a crucial development for such modeling of marine terrace sequences. Since coastal morphology can record several million years of SL history (Pedoja et al., 2014) a modeling perspective of terrace sequences could have a major impact on our understanding of SL signatures within tectonically uplifting coastlines.

6 Conclusions

Using a landscape evolution model to recreate the morphology of marine terrace sequences with a broad range of sea-level curves, allows us to 1) assess possible ages for undated marine terraces, 2) constrain the physical parameters involved in the formation of such sequences, and 3) evaluate which types of SL curves are the most consistent with the geometry of the studied sequences. In the case of the ~240 ka Xylokaastro sequence, the curves are the most consistent when interstadial highstands are relatively high, like the curves based on coral data. Contrarily, the curve based on hydraulic models appears to be more appropriate to reproduce the typical sequence morphology observed in 2.6 Ma sequences. This emphasizes the importance of

highstand elevations on such timescales, and suggests that the right choice of SL-curve might relate to the timespan/uplift rates under consideration. The combination of detailed morphological analysis of a marine terrace sequence with a careful modeling approach has the potential to provide an important new perspective on SL-cycles and tectonic uplift.

Acknowledgments, Samples, and Data

GdG, DFB, RA and RL acknowledge funding from the People Programme (Marie Skłodowska-Curie Actions) of the European Union's Seventh Framework Programme under the ITN project ALerT (Grant FP7-PEOPLE-2013-ITN number 607996). DM acknowledges financial support from the Millennium Nucleus The Seismic Cycle Along Subduction Zones funded by the Millennium Scientific Initiative (ICM) of the Chilean Government (grant 1150321) and Chilean National Fund for Development of Science and Technology (FONDECYT; grant 1181479). We thank Arthur Delorme for assistance in producing the DSM, Riccardo Caputo for sea-level curve data, Stephanie Bates for her spectral analysis code and Laurent Husson, Marco Meschis and Jennifer Robertson for fruitful discussions. Numerical computations for the DSM were performed on the S-CAPAD platform, Institut de Physique du Globe de Paris (IPGP), France. Pleiades satellite imagery was obtained through the ISIS and Tosca programs of the Centre National d'Etudes Spatiales (CNES, France) under an academic license and is not for open distribution. On request, we will provide the DSM calculated from this imagery to any academic researcher who gets approval from CNES (contact isis-pleiades@cnes.fr quoting this paper, lacassin@ipgp.fr in copy). All other data in this paper can be found in the supporting tables and references.

References

- Anderson, R. S., Densmore, A. L., & Ellis, M. A. (1999). The generation and degradation of marine terraces. *Basin Research*, *11*(1), 7–19.
- Armijo, R., Meyer, B., King, G. C. P., Rigo, A., & Papanastassiou, D. (1996). Quaternary evolution of the Corinth Rift and its implications for the Late Cenozoic evolution of the Aegean. *Geophysical Journal International*, *126*(1), 11–53.
- Bates, S. L., Siddall, M., & Waelbroeck, C. (2014). Hydrographic variations in deep ocean temperature over the mid-Pleistocene transition. *Quaternary Science Reviews*, *88*, 147–158.
- Bintanja, R., & van de Wal, R. S. W. (2008). North American ice-sheet dynamics and the onset of 100,000-year glacial cycles. *Nature*, *454*(7206), 869–872.
- Bintanja, R., van de Wal, R. S. W., & Oerlemans, J. (2005). Modelled atmospheric temperatures and global sea levels over the past million years. *Nature*, *437*(7055), 125–128.
- Bloom, A. L. (1967). Pleistocene Shorelines: A New Test of Isostasy. *GSA Bulletin*, *78*(12), 1477–1494.
- Bloom, A. L. (1971). Glacial-eustatic and isostatic controls of sea level since the last glaciation. *Late Cenozoic Glacial Ages*, 355–379.
- Bowles, C. J., & Cowgill, E. (2012). Discovering marine terraces using airborne LiDAR along the Mendocino-Sonoma coast, northern California. *Geosphere*, *8*(2), 386–402.

- Bradley, W. C. (1958). Submarine abrasion and wave-cut platforms. *GSA Bulletin*, 69(8), 967–974.
- Caputo, R. (2007). Sea-level curves: Perplexities of an end-user in morphotectonic applications. *Global and Planetary Change*, 57(3), 417–423.
- Chappell, J., & Shackleton, N. J. (1986). Oxygen isotopes and sea level. *Nature*, 324(6093), 137–140.
- Clark, P. U., Archer, D., Pollard, D., Blum, J. D., Rial, J. A., Brovkin, V., ... Roy, M. (2006). The middle Pleistocene transition: characteristics, mechanisms, and implications for long-term changes in atmospheric pCO₂. *Quaternary Science Reviews*, 25(23), 3150–3184.
- Collier, R. E. L., Leeder, M. R., Rowe, P. J., & Atkinson, T. C. (1992). Rates of tectonic uplift in the Corinth and Megara Basins, central Greece. *Tectonics*, 11(6), 1159–1167.
- De Boer, B., Van de Wal, R., Bintanja, R., Lourens, L. J., & Tuenter, E. (2010). Cenozoic global ice-volume and temperature simulations with 1-D ice-sheet models forced by benthic 18O records. *Annals of Glaciology*, 51(55), 23–33.
- De Gelder, G., Fernández-Blanco, D., Lacassin, R., Armijo, R., Delorme, A., Jara-Muñoz, J., & Melnick, D. (2015). Corinth terraces re-visited: Improved paleoshoreline determination using Pleiades-DEMs. *Geotectonic Research*, 97, 12–14.
- De Gelder, G., Fernández-Blanco, D., Melnick, D., Duclaux, G., Bell, R., Jara-Muñoz, J., ... Lacassin, R. (2017). Lithospheric flexure and rheology determined by climate cycle markers in the Corinth Rift. Preprint: <https://eartharxiv.org/4sh8e/>
- Dia, A. N., Cohen, A. S., O’Nions, R. K., & Jackson, J. A. (1997). Rates of uplift investigated through 230 Th dating in the Gulf of Corinth (Greece). *Chemical Geology*, 138(3), 171–184.
- Dufaure, J.-J., & Zamanis, A. (1979). Un vieux problème géomorphologique: les niveaux bordiers au sud du Golfe de Corinthe (An old geomorphological problem: the levels developed on the southern border of the gulf of Corinth). *Bulletin de l’Association de Géographes Français*, 56(464), 341–350.
- Elderfield, H., Ferretti, P., Greaves, M., Crowhurst, S., McCave, I. N., Hodell, D., & Piotrowski, A. M. (2012). Evolution of ocean temperature and ice volume through the mid-Pleistocene climate transition. *Science*, 337(6095), 704–709.
- Grant, K. M., Rohling, E. J., Ramsey, C. B., Cheng, H., Edwards, R. L., Florindo, F., ... Williams, F. (2014). Sea-level variability over five glacial cycles. *Nature Communications*, 5, 5076.
- Guyomard, T. S., Aïssaoui, D. M., & McNeill, D. F. (1996). Magnetostratigraphic dating of the uplifted atoll of Maré: Geodynamics of the Loyalty Ridge, SW Pacific. *Journal of Geophysical Research*, 101(B1), 601–612.
- Hearty, P. J., Hollin, J. T., Neumann, A. C., O’Leary, M. J., & McCulloch, M. (2007). Global sea-level fluctuations during the Last Interglaciation (MIS 5e). *Quaternary Science Reviews*, 26(17), 2090–2112.

- Henry, H., Regard, V., Pedoja, K., Husson, L., Martinod, J., Witt, C., & Heuret, A. (2014). Upper Pleistocene uplifted shorelines as tracers of (local rather than global) subduction dynamics. *Journal of Geodynamics*, 78, 8–20.
- Husson, L., Pastier, A.-M., Pedoja, K., Elliot, M., Paillard, D., Authemayou, C., ... Cahyarini, S. Y. (2018). Reef Carbonate Productivity During Quaternary Sea Level Oscillations. *Geochemistry, Geophysics, Geosystems*, 19(4), 1148–1164.
- Jara-Muñoz, J., Melnick, D., & Strecker, M. R. (2016). TerraceM: A MATLAB® tool to analyze marine and lacustrine terraces using high-resolution topography. *Geosphere*, 12(1), 176–195.
- Jara-Muñoz, J., Melnick, D., Zambrano, P., Rietbrock, A., González, J., Argandoña, B., & Strecker, M. R. (2017). Quantifying offshore forearc deformation and splay-fault slip using drowned Pleistocene shorelines, Arauco Bay, Chile. *Journal of Geophysical Research, Solid Earth* 122(6), 4529–4558.
- Johnston, P. (1993). The effect of spatially non-uniform water loads on prediction of sea-level change. *Geophysical Journal International*, 114(3), 615–634.
- Keraudren, B., & Sorel, D. (1987). The terraces of Corinth (Greece) — A detailed record of eustatic sea-level variations during the last 500,000 years. *Marine Geology*, 77(1), 99–107.
- Lajoie, K. R. (1986). Coastal tectonics. *Active Tectonics*.
- Lambeck, K. (1995). Late Pleistocene and Holocene sea-level change in Greece and south-western Turkey: a separation of eustatic, isostatic and tectonic contributions. *Geophysical Journal International*, 122(3), 1022–1044.
- Lambeck, K., Esat, T. M., & Potter, E.-K. (2002). Links between climate and sea levels for the past three million years. *Nature*, 419(6903), 199–206.
- Lambeck, K., Purcell, A., Johnston, P., Nakada, M., & Yokoyama, Y. (2003). Water-load definition in the glacio-hydro-isostatic sea-level equation. *Quaternary Science Reviews*, 22(2), 309–318.
- Lambeck, K., Purcell, A., Zhao, J., & Svensson, N.-O. (2010). The Scandinavian Ice Sheet: from MIS 4 to the end of the Last Glacial Maximum. *Boreas*, 39(2), 410–435.
- Lambeck, K., Purcell, A., & Dutton, A. (2012). The anatomy of interglacial sea levels: The relationship between sea levels and ice volumes during the Last Interglacial. *Earth and Planetary Science Letters*, 315, 4–11.
- Lambeck, K., Rouby, H., Purcell, A., Sun, Y., & Sambridge, M. (2014). Sea level and global ice volumes from the Last Glacial Maximum to the Holocene. *Proceedings of the National Academy of Sciences of the United States of America*, 111(43), 15296–15303.
- Lambeck, K., Purcell, A., & Zhao, S. (2017). The North American Late Wisconsin ice sheet and mantle viscosity from glacial rebound analyses. *Quaternary Science Reviews*, 158, 172–210.
- Lea, D. W., Martin, P. A., Pak, D. K., & Spero, H. J. (2002). Reconstructing a 350ky history of sea level using planktonic Mg/Ca and oxygen isotope records from a Cocos Ridge core. *Quaternary Science Reviews*, 21(1), 283–293.
- Leeder, M. R., Portman, C., Andrews, J. E., Collier, R. E. L., Finch, E., Gawthorpe, R. L., ... Rowe, P. (2005). Normal faulting and crustal deformation, Alkyonides Gulf and Perachora

peninsula, eastern Gulf of Corinth rift, Greece. *Journal of the Geological Society*, 162(3), 549–561.

Meco, J., Scaillet, S., Guillou, H., Lomoschitz, A., Carlos Carracedo, J., Ballester, J., ... Cilleros, A. (2007). Evidence for long-term uplift on the Canary Islands from emergent Mio–Pliocene littoral deposits. *Global and Planetary Change*, 57(3), 222–234.

Melnick, D. (2016). Rise of the central Andean coast by earthquakes straddling the Moho. *Nature Geoscience*, 9(5), 401–407.

Merritts, D., & Bull, W. B. (1989). Interpreting Quaternary uplift rates at the Mendocino triple junction, northern California, from uplifted marine terraces. *Geology*, 17(11), 1020–1024.

Moretti, I., Lykousis, V., Sakellariou, D., Reynaud, J.-Y., Benziane, B., & Prinzhofer, A. (2004). Sedimentation and subsidence rate in the Gulf of Corinth: what we learn from the Marion Dufresne's long-piston coring. *Comptes Rendus: Geoscience*, 336(4), 291–299.

Murray-Wallace, C. V. (2002). Pleistocene coastal stratigraphy, sea-level highstands and neotectonism of the southern Australian passive continental margin—a review. *Journal of Quaternary Science*, 17(5-6), 469–489.

Murray-Wallace, C. V., & Woodroffe, C. D. (2014). *Quaternary Sea-Level Changes: A Global Perspective*. Cambridge University Press.

Nakada, M., & Lambeck, K. (1989). Late Pleistocene and Holocene sea-level change in the Australian region and mantle rheology. *Geophysical Journal International*, 96(3), 497–517.

Pedoja, K., Husson, L., Regard, V., Cobbold, P. R., Ostanciaux, E., Johnson, M. E., ... Delcaillau, B. (2011). Relative sea-level fall since the last interglacial stage: Are coasts uplifting worldwide? *Earth-Science Reviews*, 108(1), 1–15.

Pedoja, K., Husson, L., Johnson, M. E., Melnick, D., Witt, C., Pochat, S., ... Garestier, F. (2014). Coastal staircase sequences reflecting sea-level oscillations and tectonic uplift during the Quaternary and Neogene. *Earth-Science Reviews*, 132, 13–38.

Pedoja, K., Jara-Muñoz, J., De Gelder, G., Robertson, J., Meschis, M., Fernandez-Blanco, D., ... Pinel, B. (2018a). Neogene-Quaternary slow coastal uplift of Western Europe through the perspective of sequences of strandlines from the Cotentin Peninsula (Normandy, France). *Geomorphology*, 303, 338–356.

Pedoja, K., Husson, L., Bezos, A., Pastier, A.-M., Imran, A. M., Arias-Ruiz, C., ... Choblet, G. (2018b). On the long-lasting sequences of coral reef terraces from SE Sulawesi (Indonesia): Distribution, formation, and global significance. *Quaternary Science Reviews*, 188, 37–57.

Perissoratis, C., Piper, D. J. W., & Lykousis, V. (2000). Alternating marine and lacustrine sedimentation during late Quaternary in the Gulf of Corinth rift basin, central Greece. *Marine Geology*, 167(3–4), 391–411.

Pierini, F., Demarchi, B., Turner, J., & Penkman, K. (2016/2). Pecten as a new substrate for IcpD dating: The quaternary raised beaches in the Gulf of Corinth, Greece. *Quaternary Geochronology*, 31, 40–52.

- Quartau, R., Trenhaile, A. S., Mitchell, N. C., & Tempera, F. (2010). Development of volcanic insular shelves: Insights from observations and modelling of Faial Island in the Azores Archipelago. *Marine Geology*, 275(1), 66–83.
- Railsback, L. B., Gibbard, P. L., Head, M. J., Voarintsoa, N. R. G., & Toucanne, S. (2015). An optimized scheme of lettered marine isotope substages for the last 1.0 million years, and the climatostratigraphic nature of isotope stages and substages. *Quaternary Science Reviews*, 111, 94–106.
- Regard, V., Pedoja, K., De La Torre, I., Saillard, M., Cortés-Aranda, J., & Nexer, M. (2017). Geometrical trends within sequences of Pleistocene marine terraces: selected examples from California, Peru, Chile and New-Zealand. *Zeitschrift Fur Geomorphologie*, 61(1), 53–73.
- Roberts, G. P., Meschis, M., Houghton, S., Underwood, C., & Briant, R. M. (2013). The implications of revised Quaternary palaeoshoreline chronologies for the rates of active extension and uplift in the upper plate of subduction zones. *Quaternary Science Reviews*, 78, 169–187.
- Rohling, E. J., Foster, G. L., Grant, K. M., Marino, G., Roberts, A. P., Tamisiea, M. E., & Williams, F. (2014). Sea-level and deep-sea-temperature variability over the past 5.3 million years. *Nature*, 508(7497), 477–482.
- Rohling, E. J., Grant, K., Bolshaw, M., Roberts, A. P., Siddall, M., Hemleben, C., & Kucera, M. (2009). Antarctic temperature and global sea level closely coupled over the past five glacial cycles. *Nature Geoscience*, 2(7), 500.
- Shackleton, N. J. (2000). The 100,000-year ice-Age cycle identified and found to lag temperature, carbon dioxide, and orbital eccentricity. *Science*, 289(5486), 1897–1902.
- Shakun, J. D., Lea, D. W., Lisiecki, L. E., & Raymo, M. E. (2015). An 800-kyr record of global surface ocean $\delta^{18}\text{O}$ and implications for ice volume-temperature coupling. *Earth and Planetary Science Letters*, 426, 58–68.
- Shaw, B., Ambraseys, N. N., England, P. C., Floyd, M. A., Gorman, G. J., Higham, T., ... Piggott, M. D. (2008). Eastern Mediterranean tectonics and tsunami hazard inferred from the AD 365 earthquake. *Nature Geoscience*, 1(4), 268.
- Siddall, M., Hönisch, B., Waelbroeck, C., & Huybers, P. (2010). Changes in deep Pacific temperature during the mid-Pleistocene transition and Quaternary. *Quaternary Science Reviews*, 29(1), 170–181.
- Simms, A. R., Rouby, H., & Lambeck, K. (2016). Marine terraces and rates of vertical tectonic motion: The importance of glacio-isostatic adjustment along the Pacific coast of central North America. *GSA Bulletin*, 128(1-2), 81–93.
- Spratt, R. M., & Lisiecki, L. E. (2016). A Late Pleistocene sea level stack. *Climate of the Past*, 12(4), 1079.
- Strobl, M., Hetzel, R., Fassoulas, C., & Kubik, P. W. (2014). A long-term rock uplift rate for eastern Crete and geodynamic implications for the Hellenic subduction zone. *Journal of Geodynamics*, 78, 21–31.
- Suess, E. (1888). *Das Antlitz der Erde, II. Tempsky, Wien*, 1–723.
- Sunamura, T. (1992). *Geomorphology of rocky coasts* (Vol. 3). John Wiley & Son Ltd.

Waelbroeck, C., Labeyrie, L., Michel, E., Duplessy, J. C., McManus, J. F., Lambeck, K., ... Labracherie, M. (2002). Sea-level and deep water temperature changes derived from benthic foraminifera isotopic records. *Quaternary Science Reviews*, 21(1), 295–305.

Walcott, R. I. (1972). Past Sea Levels, Eustasy and Deformation of the Earth. *Quaternary Research*, 2(1), 1–14.

Yamato, P., Husson, L., Becker, T. W., & Pedoja, K. (2013). Passive margins getting squeezed in the mantle convection vice. *Tectonics*, 32(6).

Yildirim, C., Melnick, D., Ballato, P., Schildgen, T. F., Echtler, H., Erginal, A. E., ... Strecker, M. R. (2013). Differential uplift along the northern margin of the Central Anatolian Plateau: inferences from marine terraces. *Quaternary Science Reviews*, 81, 12–28.

Zeuner, F. E. (1952). Pleistocene Shore-lines. *Geologische Rundschau: Zeitschrift Fur Allgemeine Geologie*, 40(1), 39–50.

The Influence of Sea-Level Curves on Modeled Marine Terrace Sequences

Gino de Gelder¹, Julius Jara-Muñoz², Daniel Melnick³, David Fernández-Blanco¹, Hélène Rouby¹, Kevin Pedoja⁴, Rolando Armijo¹ and Robin Lacassin¹

¹Institut de Physique du Globe de Paris, Sorbonne Paris Cité, Univ. Paris Diderot, UMR 7154 CNRS, F-75005 Paris, France. ²Institut für Erd- und Umweltwissenschaften, Universität Potsdam, Karl-Liebknecht-Strasse 24, 14476 Potsdam, Germany. ³Instituto de Ciencias de la Tierra, Universidad Austral de Chile, 567 Valdivia, Chile ⁴Laboratoire de Morphodynamique Continentale et Côtière, CNRS, Université de Caen, 14000 Caen, France.

Contents of this file

Figures S1 to S6
Table S1

Additional Supporting Information (File uploaded separately)

Dataset S1. Swath profiles used to determine the position and elevation of marine terrace shoreline angles. Profiles show maximum and minimum topography, selected points on the terrace and paleocliff, and an estimate of the shoreline angle elevation. H1-H20 are profiles of the Holocene terrace, strongly affected by manmade structures

Introduction

Figures S1 to S4 and Dataset S1 provide supporting information on the detailed analysis of the Xylokastro marine terrace sequence, whereas Figures S5 and S6 provide supporting information on the modeling the Mid-Pleistocene Transition. Table S1 provides details about the used sea-level curves in this study.

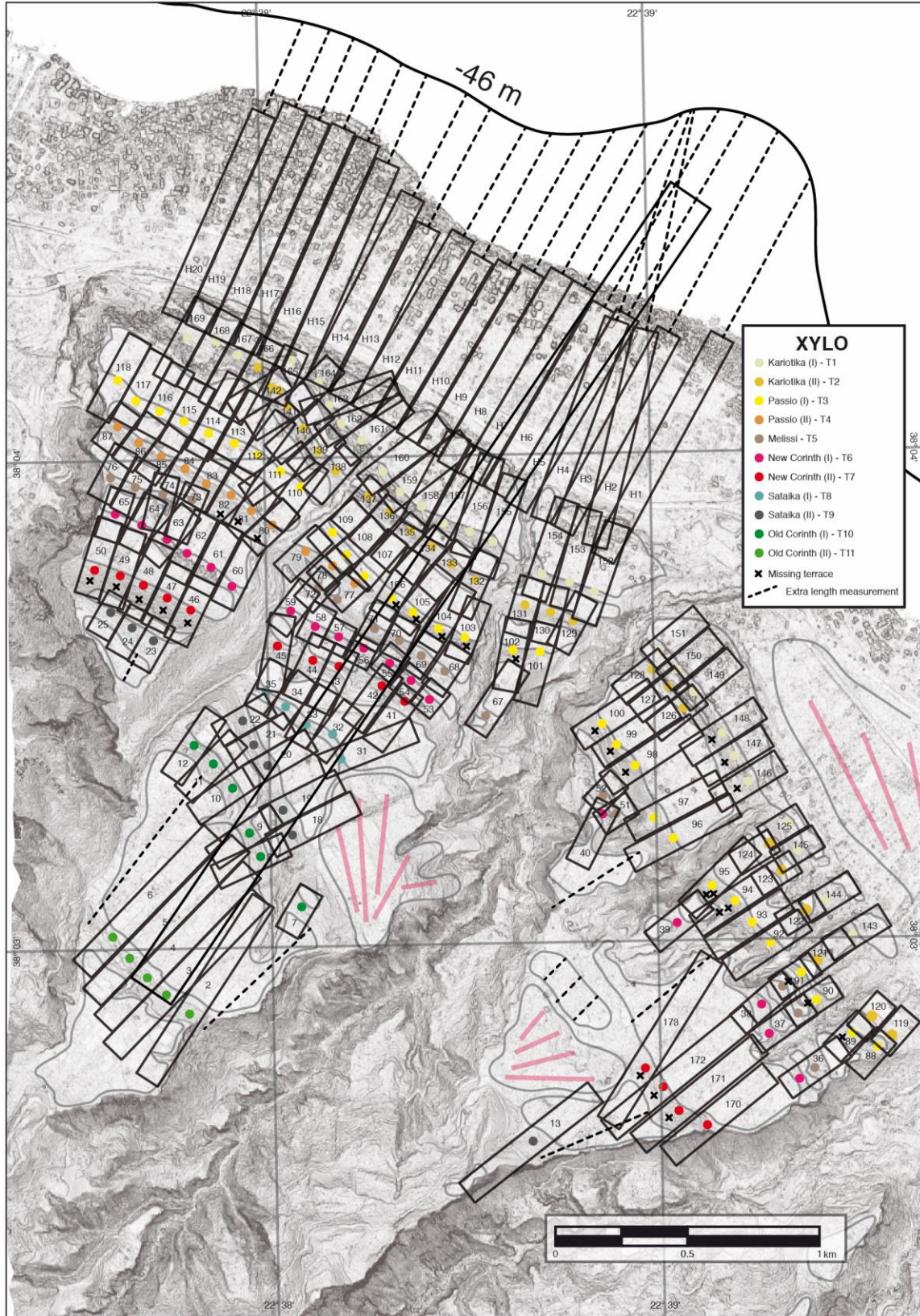


Figure S1. (Previous page) Locations of the swath profiles used to determine the position and elevation of the fossil shoreline angles as well as the width of the successive marine terraces at Xylokastro (S Corinth Gulf, Greece). Map gives location and numbering of swath profiles of Dataset S1 on a slope-map of the Pleiades DSM, and the determined shoreline angles (dots). To calculate average widths, we included a 0-m width measurement at locations where some individual terraces are missing in the sequence, and we added width measurements at locations with terrace width indications without shoreline angles.

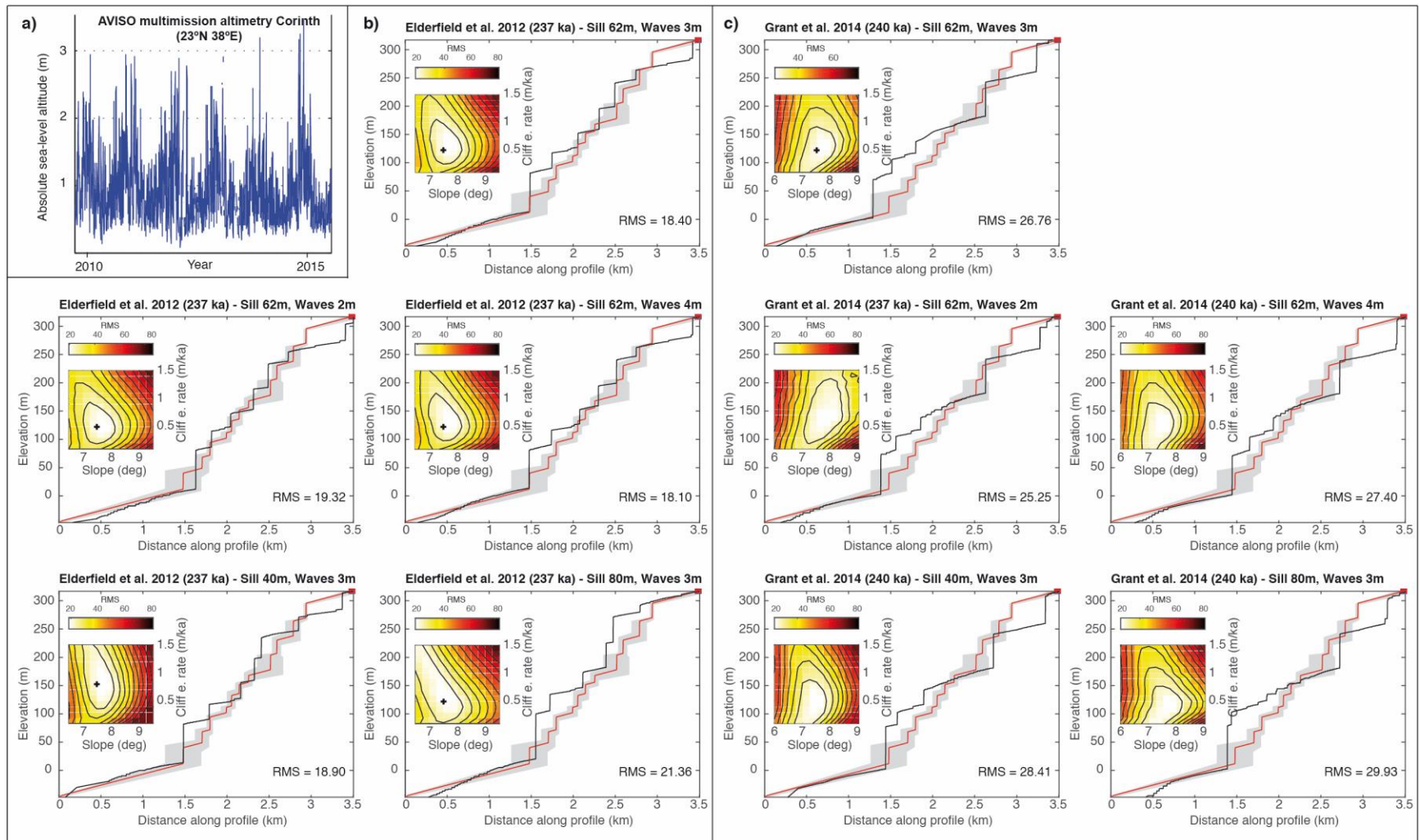
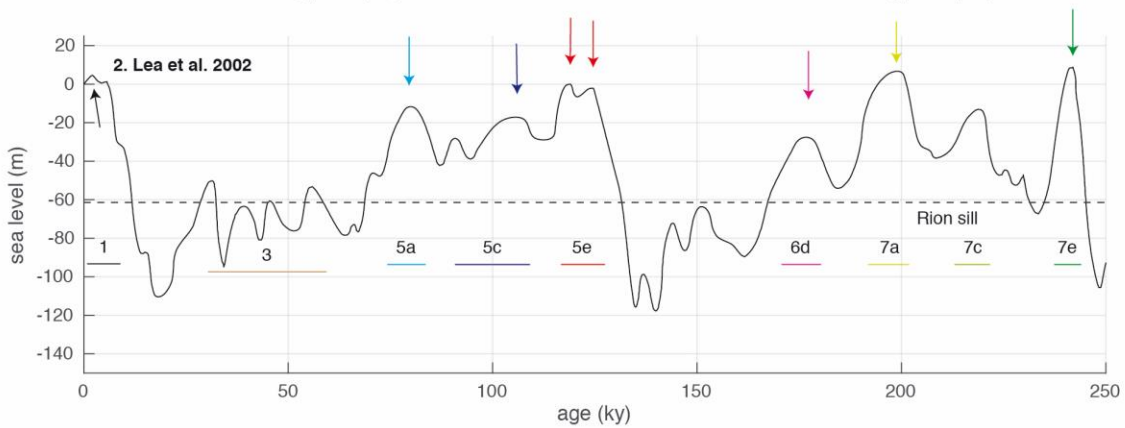
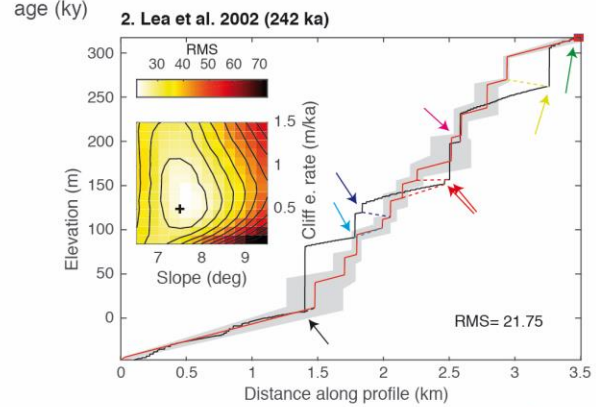
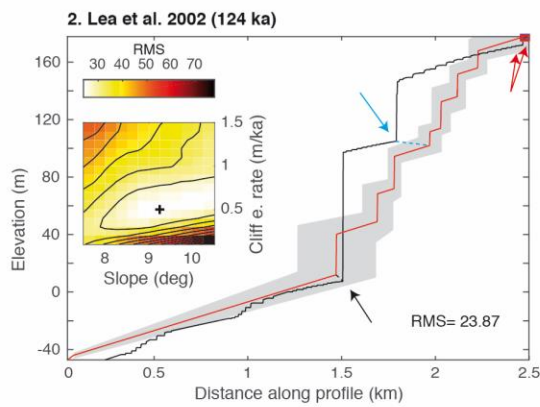
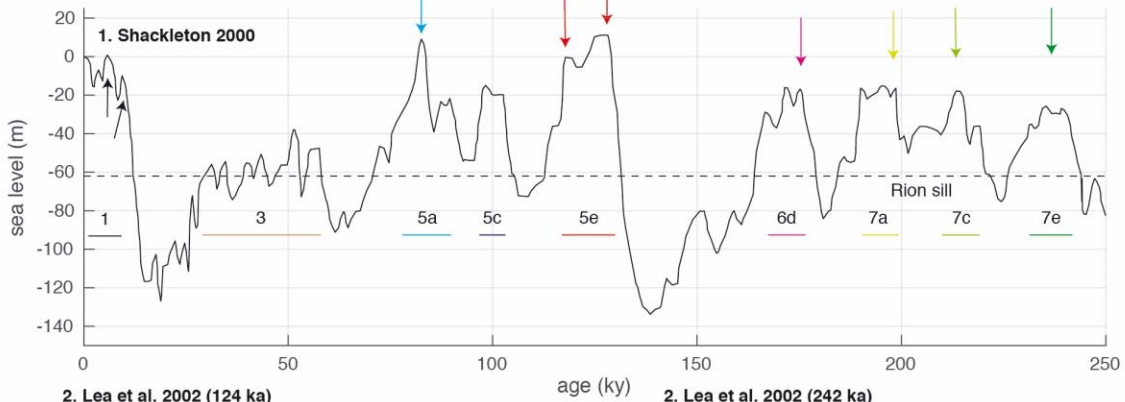
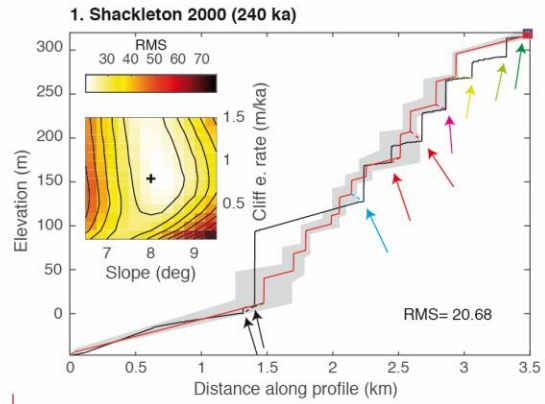
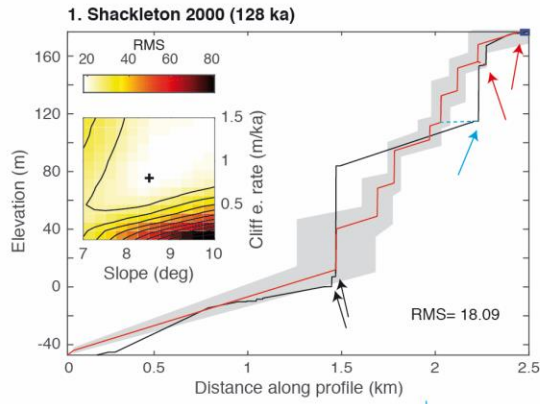
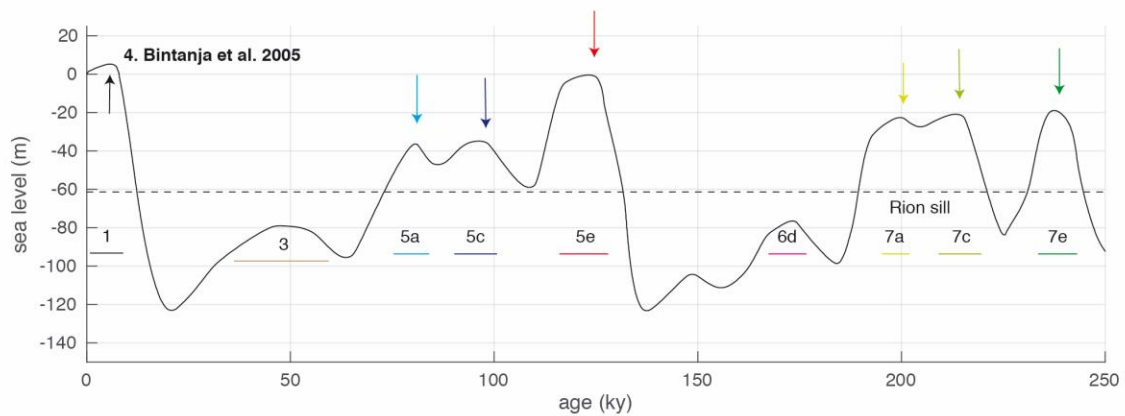
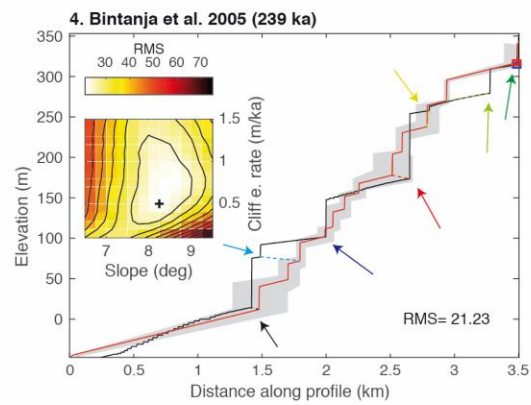
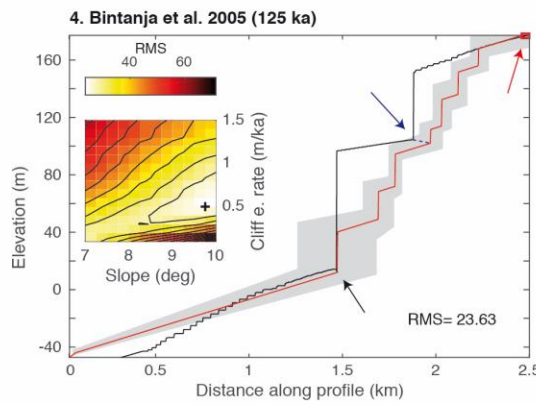
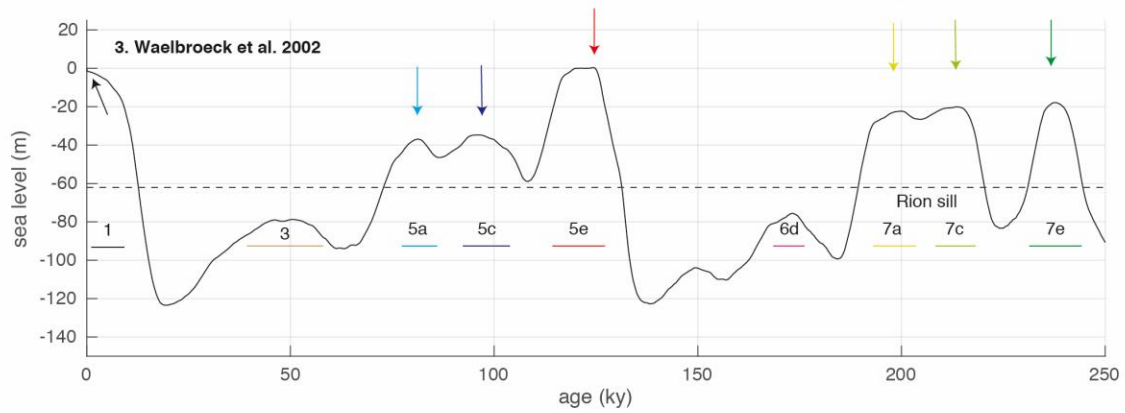
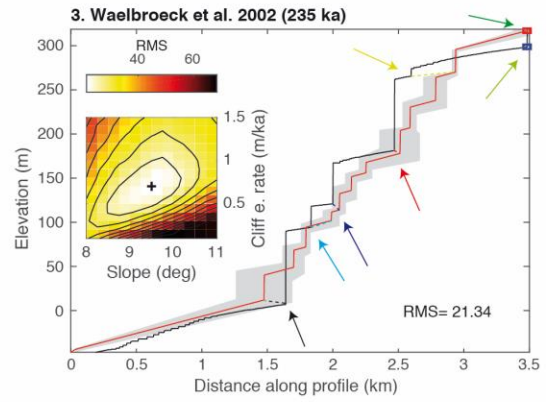
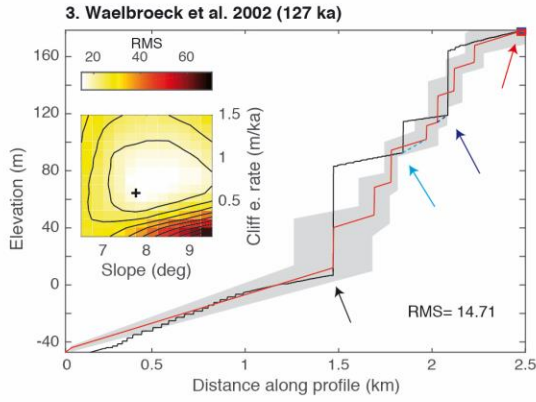
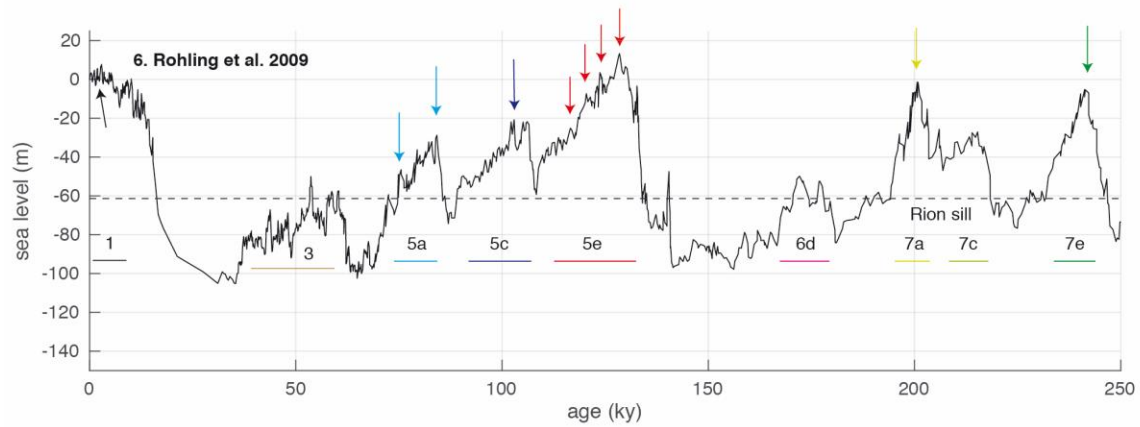
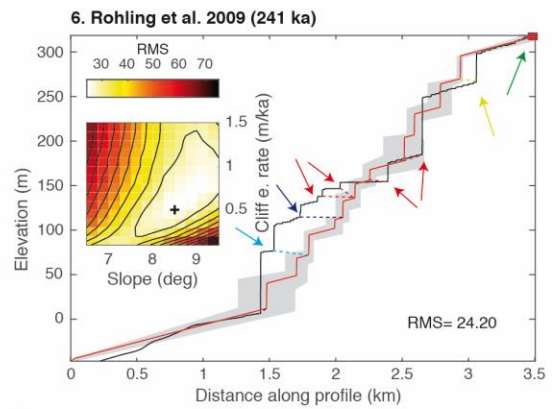
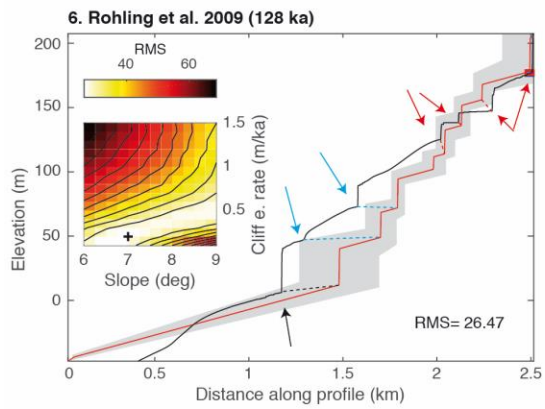
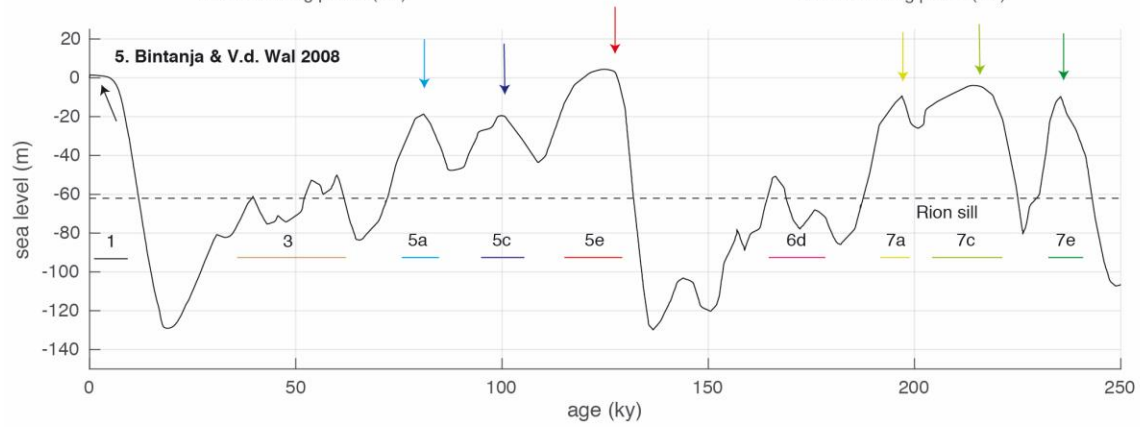
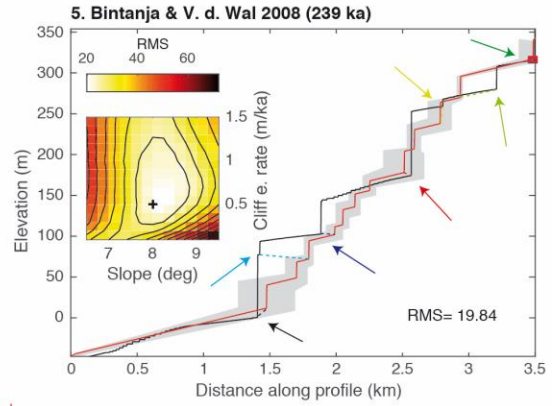
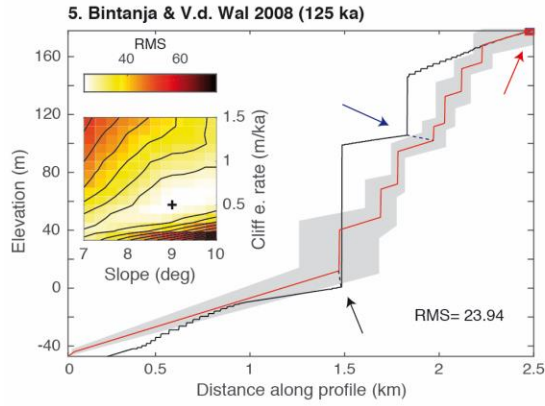
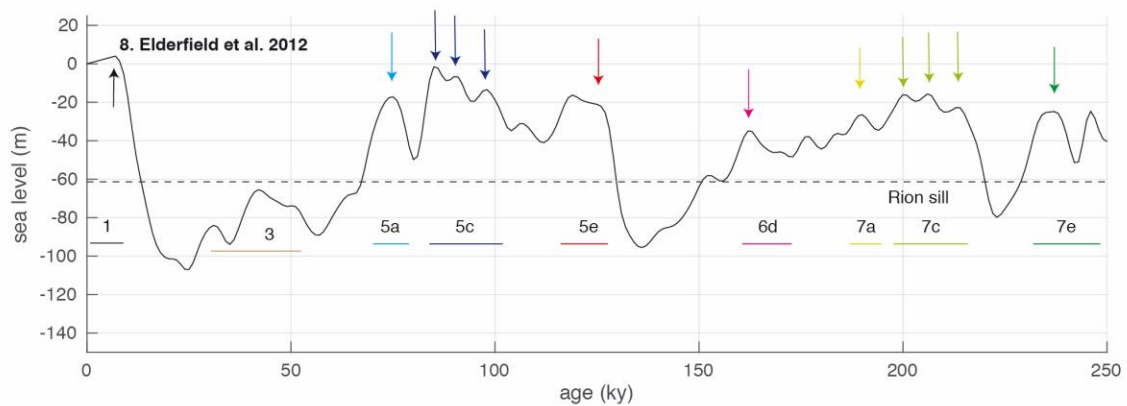
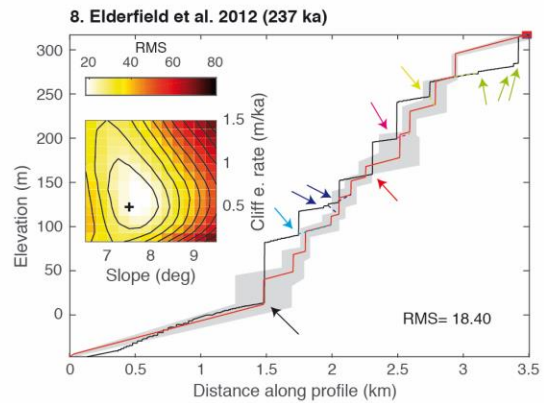
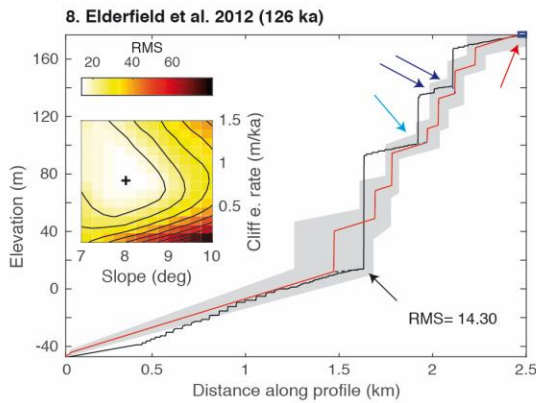
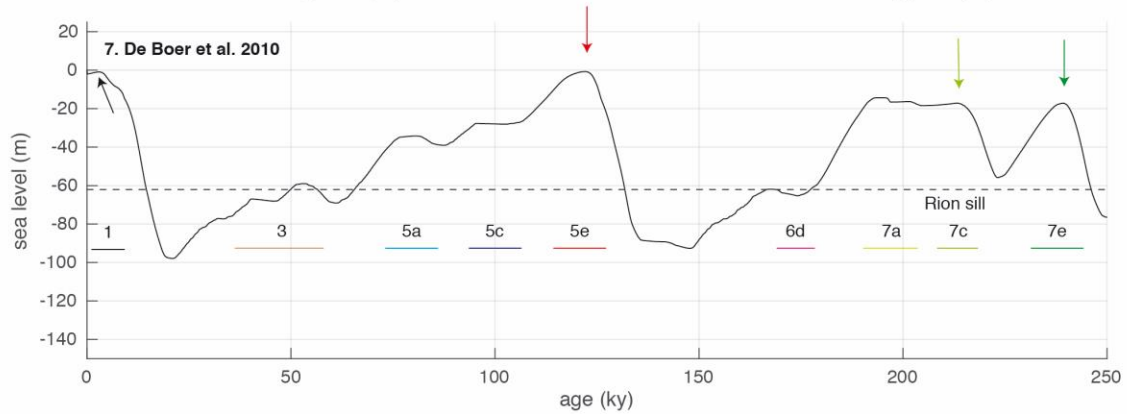
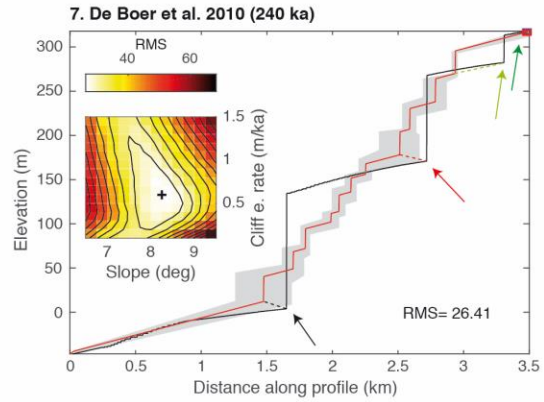
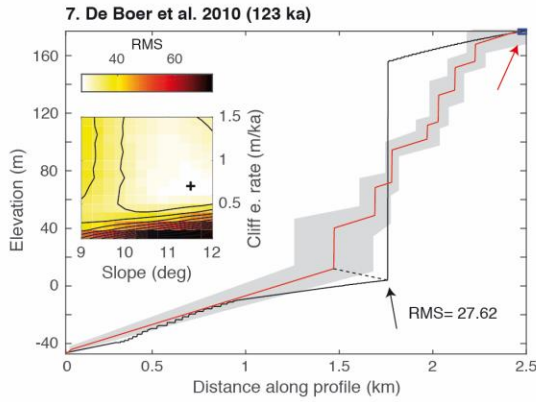


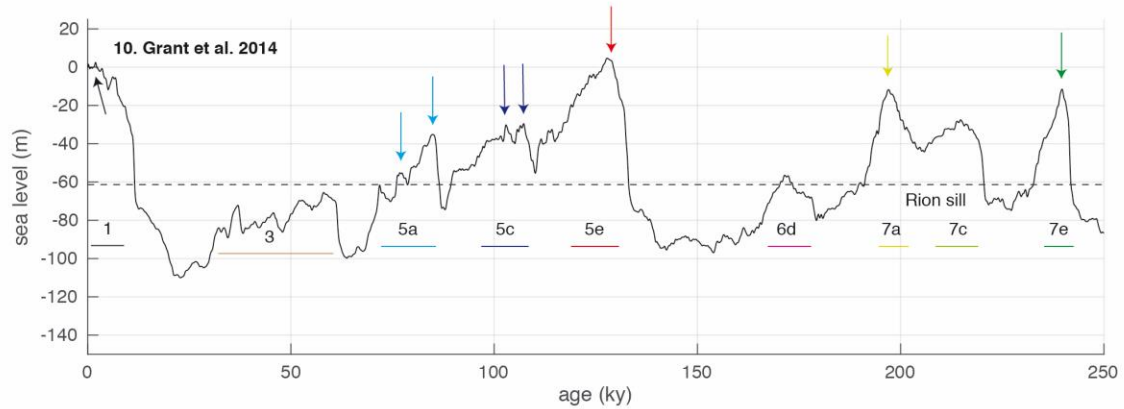
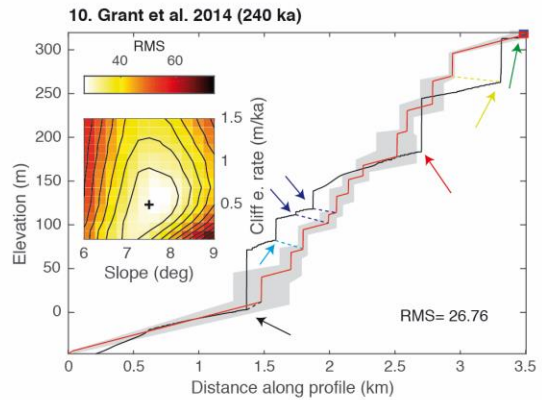
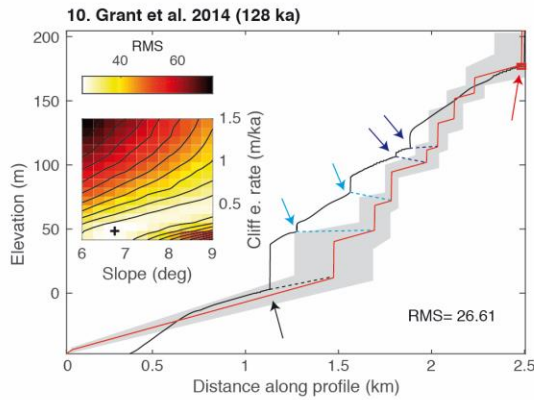
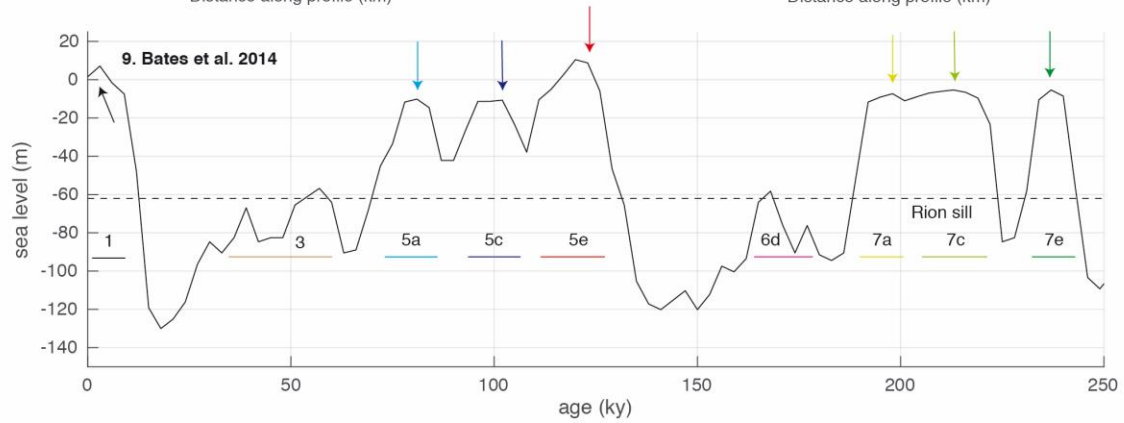
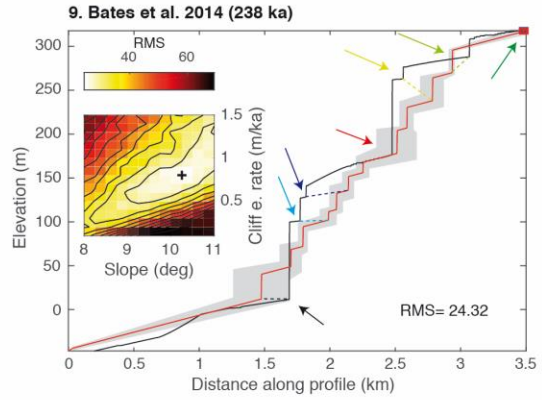
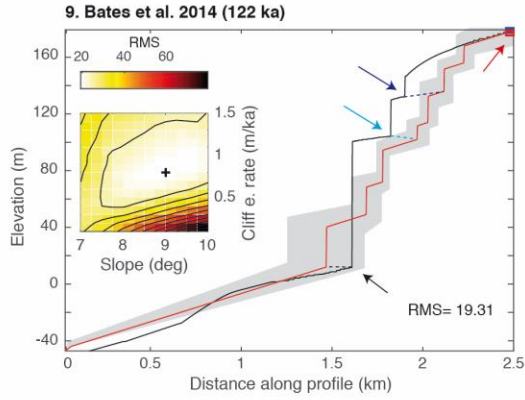
Figure S2. (a) AVISO multi-mission altimetry data for the coordinates of Corinth (23°N 38°E) between 2010-2015, indicating recorded wave heights. (b) and (c) Sensitivity tests for the curves of Elderfield et al. (2012) and Grant et al. (2014), respectively, to show the effect of using different wave heights and sill depths over ~240 ka modeling of the Xylokastro sequence.

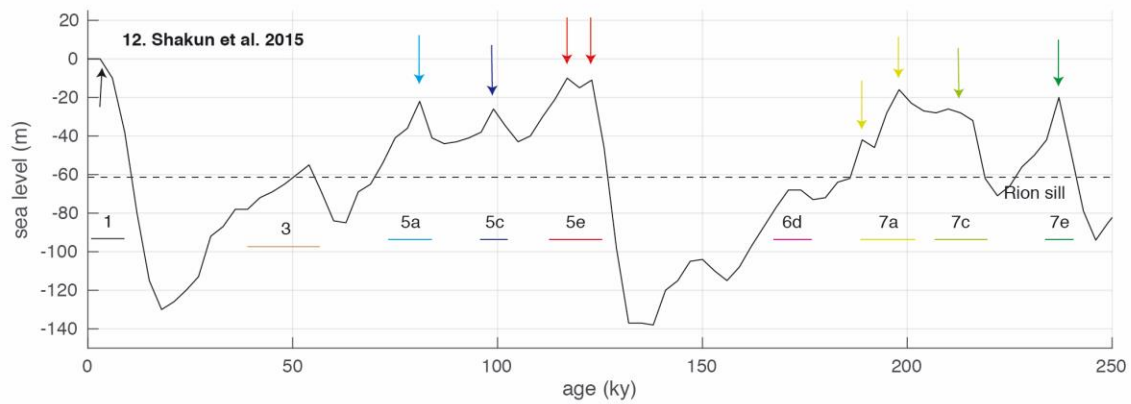
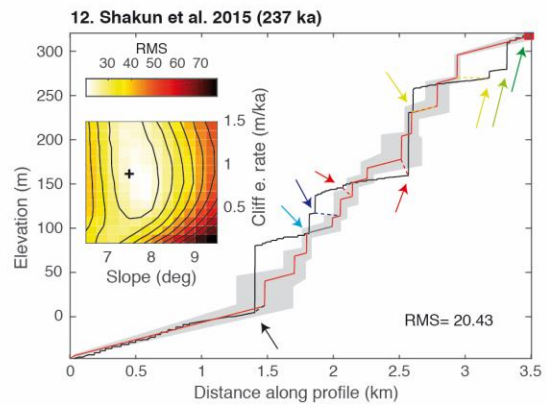
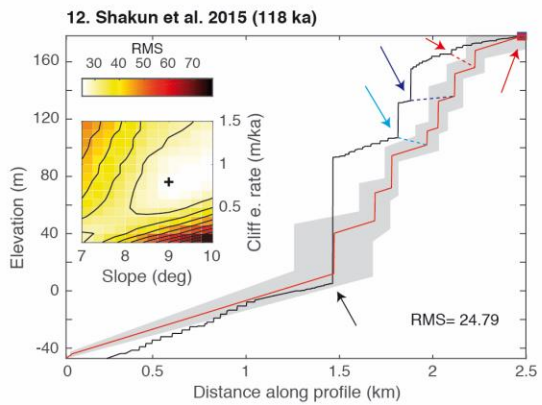
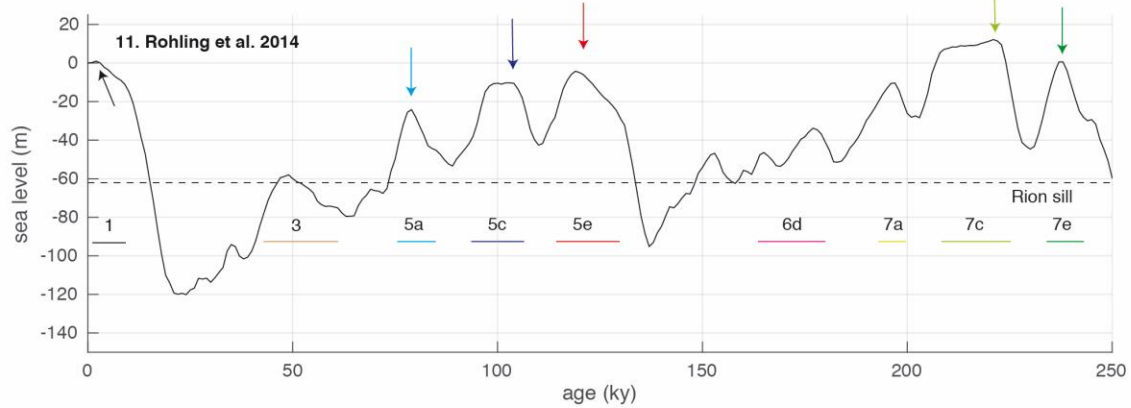
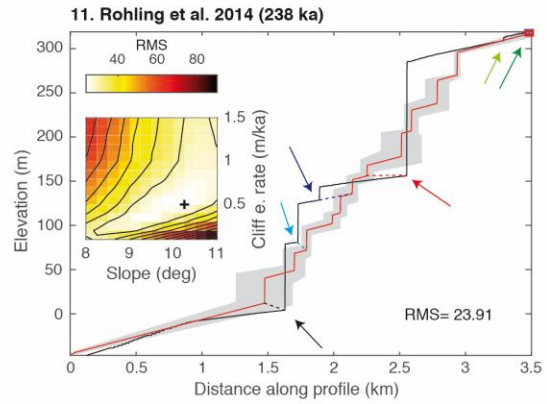
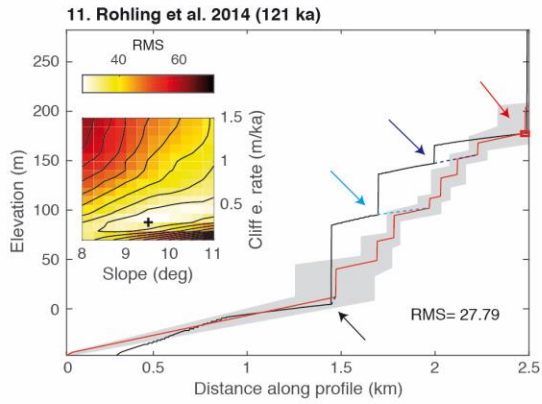












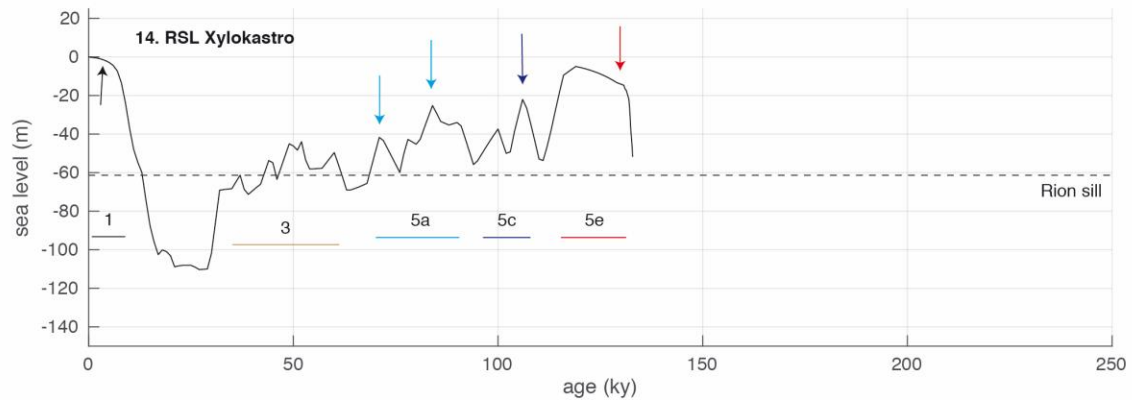
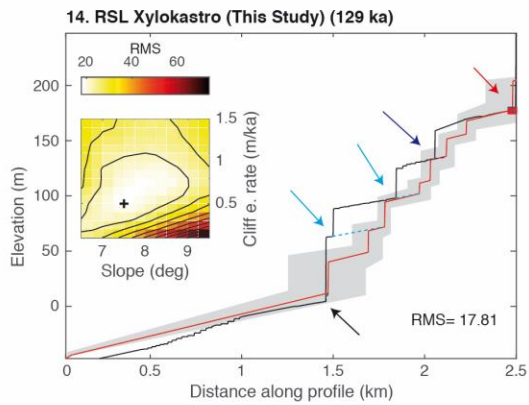
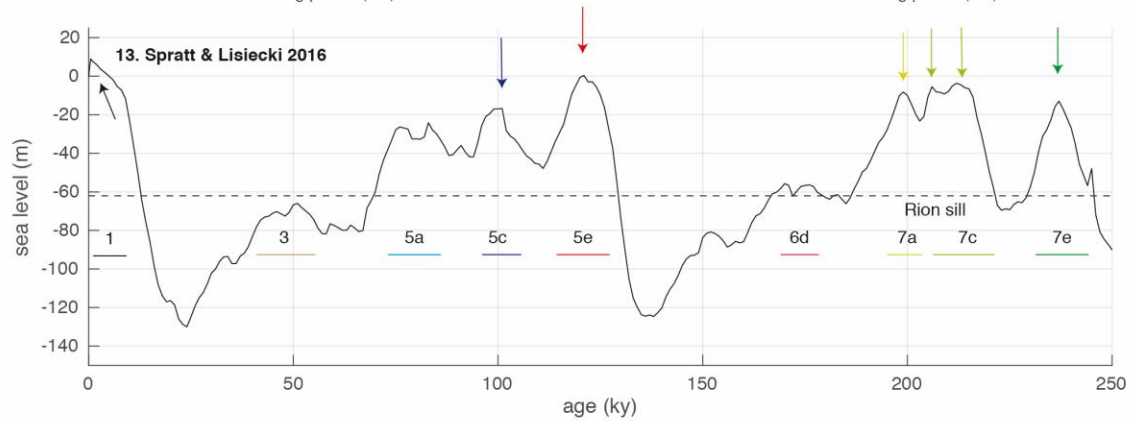
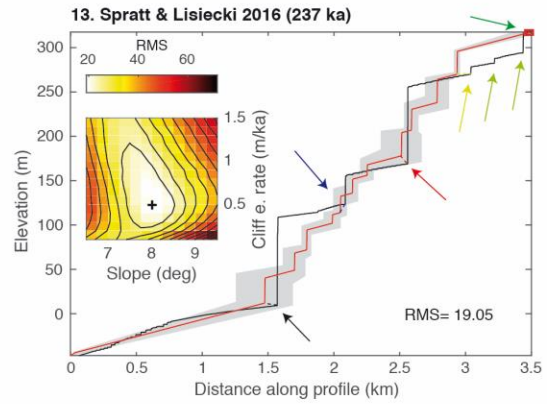
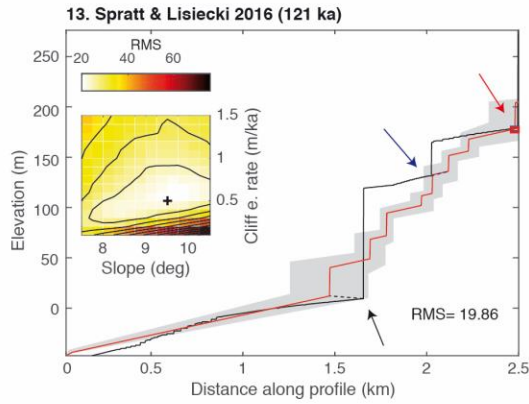


Figure S3. (Previous seven pages) Different SL curves used for modeling the sequence of marine terraces at Xylokastro (S Gulf of Corinth, Greece), and the lowest RMS misfit results on two timescales. Arrows indicate modeled terraces on both the profile and the SL curves. Dashed lines connecting shoreline angle of modeled and observed shoreline angles indicate the correlation used for Fig. 2b.

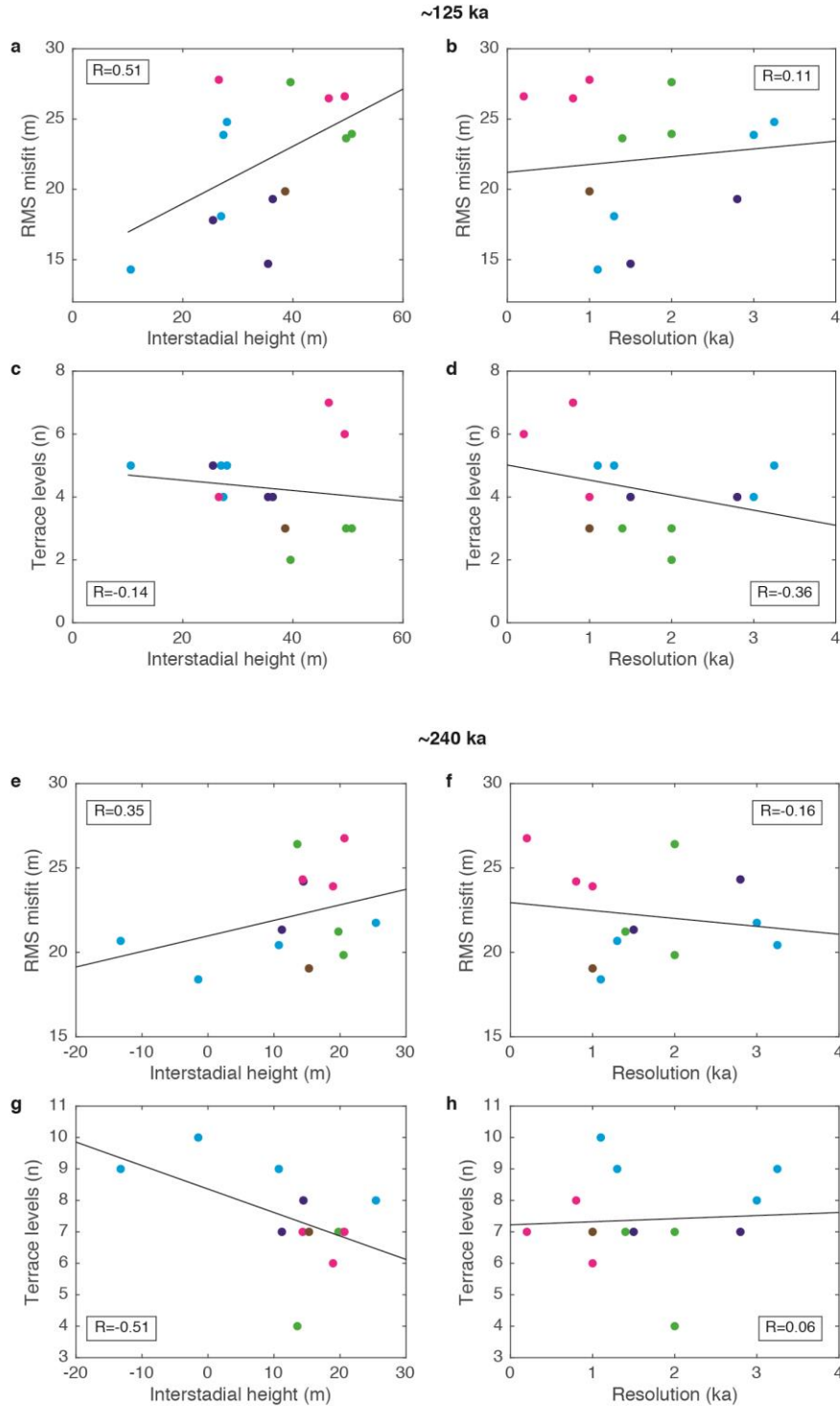


Figure S4. Correlations for the analysis of the Xylokaastro sequence, between average interstadial highstand elevation and resolution of the SL-curves on one hand, and the RMS misfit and amount of terrace levels on the other hand. Average interstadial highstand elevations (MIS 3, 5a, 5c, 6, 7a, 7c; Fig. 1d) are relative to MIS 5e and MIS 7e

highstands for ~ 125 ka and ~ 240 ka respectively. R is the correlation coefficient between the two variables.

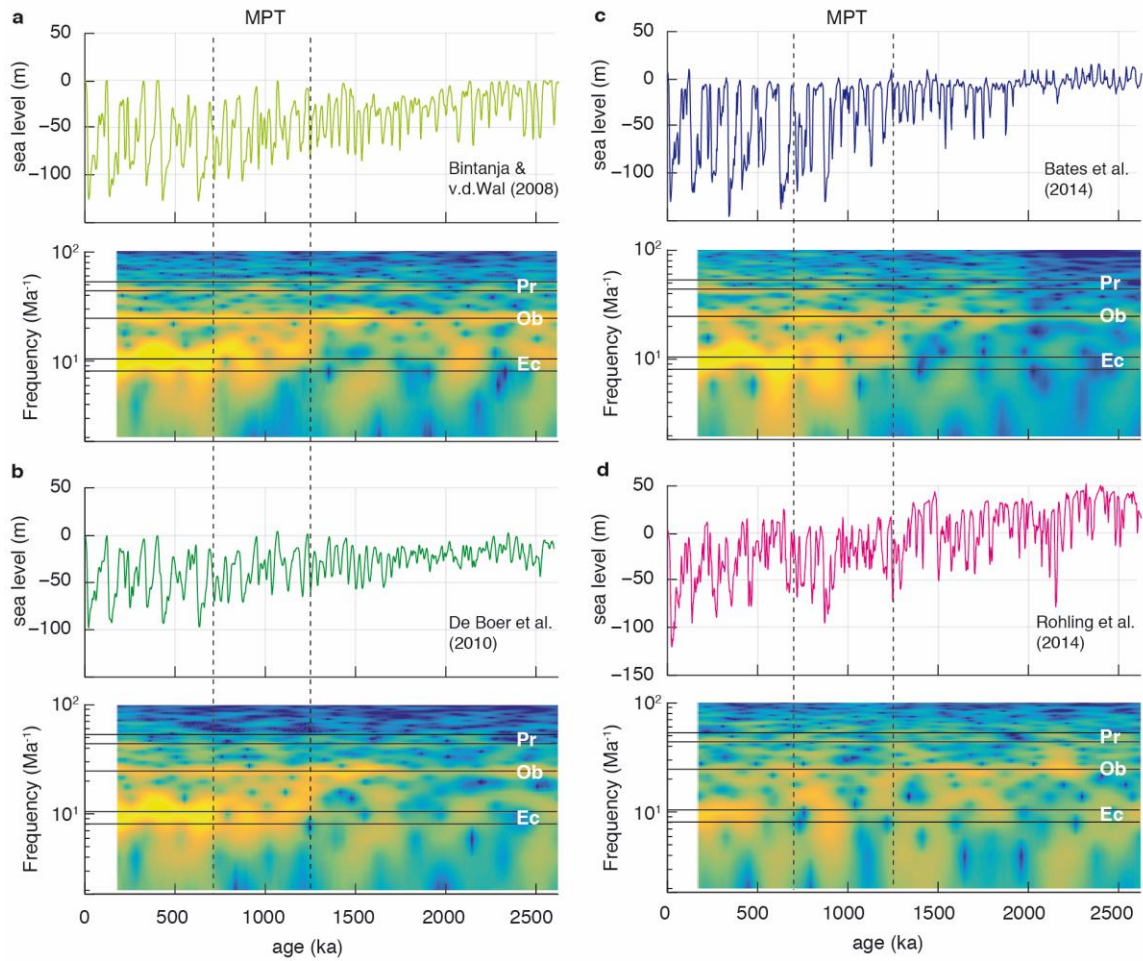


Figure S5. Spectrograms for Quaternary time-scale sea-level curves. For each SL curve, spectrograms indicate the relative power of precession (~23 ka), obliquity (~41 ka) and eccentricity (~100 ka) cycles over the past 2.6 Ma. Following Siddall et al. (2010) and Bates et al. (2014), we first applied a high-pass Butterworth filter with a 350 ka window, and produced spectrograms using a Fourier transform with a 350 ka window and 349 ka overlap.

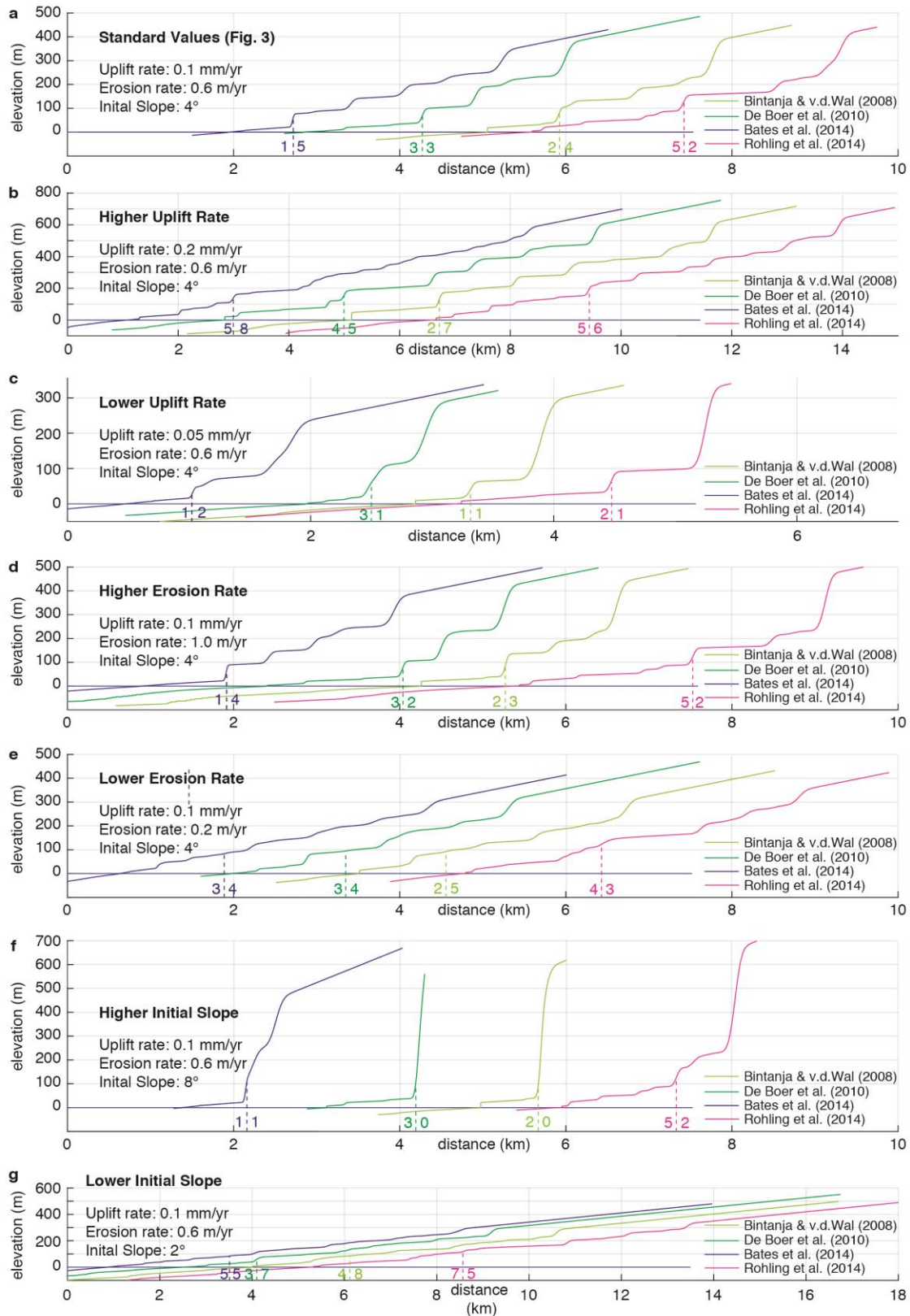


Figure S6. Extra tests on 2.6 Ma timescales, varying uplift rates, erosion rates and initial

slope. Dashed lines indicate the Mid-Pleistocene Transition (MPT); colored numbers next to it indicate the amount of terraces/rasas formed before and after the MPT.

Publication	Duration (ka)	Location	Average Resolution original data (ka)	Method
1. Shackleton 2000	400	Equatorial Pacific	1.3	$\delta^{18}\text{O}$ – temperature correction other proxy
2. Lea et al 2002	360	Cocos ridge	3.0	$\delta^{18}\text{O}$ – temperature correction other proxy
3. Waelbroeck et al 2002	430	Equatorial Pacific & N-Atlantic	1.5 (best 0.3)	$\delta^{18}\text{O}$ – coral regression
4. Bintanja et al 2005	1070	Global stack	1.4 (best 1)	Inverse ice volume model
5. Bintanja & V.d. Wal 2008	3000	Global stack	2.0 (best 1)	Inverse ice volume model
6. Rohling et al 2009	520	Red Sea	0.8 (best 0.3)	Hydraulic control models of semi-isolated basins
7. De Boer et al 2010	35000	Global stack	2.0 (best 1)	Inverse ice volume model
8. Elderfield et al 2012	1575	South Pacific	1.1	$\delta^{18}\text{O}$ – temperature correction other proxy
9. Bates et al 2014	5000	Equatorial Pacific*	2.8 (best 1.275)	$\delta^{18}\text{O}$ – coral regression
10. Grant et al 2014	500	Red Sea	0.2	Hydraulic control models of semi-isolated basins
11. Rohling et al 2014	5300	Mediterranean	1.0	Hydraulic control models of semi-isolated basins
12. Shakun et al 2015	800	Global stack	3.25 (best 1.5)	$\delta^{18}\text{O}$ – temperature correction other proxy
13. Spratt & Lisiecki 2016	800	Global stack	1.0	PCA on 7 existing records
14. This study	130	Local GIA-corrected		GIA-corrected, observation-calibrated ice volume models

* Out of the 10 SL curves in Bates et al. (2014) this was used as their reference curve for comparisons

Table S1. The different SL curves used in this study.